



# Barley GRIK1-SnRK1 kinases subvert a viral virulence protein to upregulate antiviral RNAi and inhibit infection

Huaibing Jin<sup>1,2,†</sup> , Xinyun Han<sup>2,†</sup>, Zhaohui Wang<sup>1,†</sup>, Yilin Xie<sup>3,4</sup> , Kunpu Zhang<sup>1</sup> , Xiaoge Zhao<sup>2</sup>, Lina Wang<sup>1</sup>, Jin Yang<sup>1</sup>, Huiyun Liu<sup>1</sup>, Xiang Ji<sup>1</sup>, Lingli Dong<sup>2</sup> , Hongyuan Zheng<sup>1</sup>, Weijuan Hu<sup>2</sup>, Yan Liu<sup>5</sup>, Xifeng Wang<sup>5</sup> , Xueping Zhou<sup>5</sup>, Yijing Zhang<sup>3</sup>, Weiqiang Qian<sup>6</sup> , Wenming Zheng<sup>7</sup> , Qianhua Shen<sup>2,\*</sup> , Mingyue Gou<sup>1,\*\*</sup> & Daowen Wang<sup>1,2,7,8,\*\*\*</sup>

## Abstract

Viruses often usurp host machineries for their amplification, but it remains unclear if hosts may subvert virus proteins to regulate viral proliferation. Here, we show that the 17K protein, an important virulence factor conserved in barley yellow dwarf viruses (BYDVs) and related poleroviruses, is phosphorylated by host GRIK1-SnRK1 kinases, with the phosphorylated 17K (P17K) capable of enhancing the abundance of virus-derived small interfering RNAs (vsiRNAs) and thus antiviral RNAi. Furthermore, P17K interacts with barley small RNA-degrading nuclease 1 (HvSDN1) and impedes HvSDN1-catalyzed vsiRNA degradation. Additionally, P17K weakens the HvSDN1-HvAGO1 interaction, thus hindering HvSDN1 from accessing and degrading HvAGO1-carried vsiRNAs. Importantly, transgenic expression of 17K phosphomimetics (17K<sup>5D</sup>), or genome editing of *SDN1*, generates stable resistance to BYDV through elevating vsiRNA abundance. These data validate a novel mechanism that enhances antiviral RNAi through host subversion of a viral virulence protein to inhibit SDN1-catalyzed vsiRNA degradation and suggest new ways for engineering BYDV-resistant crops.

**Keywords** antiviral RNAi; BYDV; small RNA-degrading enzyme; SnRK1; wheat

**Subject Categories** Microbiology, Virology & Host Pathogen Interaction; Plant Biology; RNA Biology

**DOI** 10.15252/emboj.2021110521 | Received 23 December 2021 | Revised 25 May 2022 | Accepted 3 June 2022 | Published online 5 August 2022

The EMBO Journal (2022) 41: e110521

## Introduction

Viruses are ubiquitous pathogens of cellular organisms, and frequently cause serious diseases in humans, livestock, and agricultural crops. As molecular parasites with small and compact genomes, viruses often usurp host resources for their proliferation. To combat viral infections, hosts have evolved a myriad of defense strategies including antiviral RNA interference (RNAi). Antiviral RNAi, guided by virus-derived small interfering RNAs (vsiRNAs), is fundamentally important for plants, animals, and fungi to control virus proliferation and viral load in infected cells (Fire *et al.*, 1998; Baulcombe, 2004; Guo *et al.*, 2019). This conserved antiviral defense requires sufficient production and accumulation of vsiRNAs and the corrected assembly and function of RNA-induced silencing complex (RISC). However, viruses encode potent suppressors of gene silencing (VSRs), which can disrupt the key steps of RNA silencing pathway, resulting in the suppression of antiviral RNAi (Guo *et al.*, 2019; Li & Wang, 2019).

It is now clear that VSRs use a variety of strategies to suppress host antiviral RNAi. For example, a number of VSRs encoded by plant, animal, or insect viruses, including the NS3 VSR of rice stripe virus, the VSRs of several mammalian viruses, and the 1A VSR of *Drosophila C* virus, can bind viral dsRNAs and impair their processing into vsiRNAs

- 1 State Key Laboratory of Wheat and Maize Crop Science, College of Agronomy, National Wheat Innovation Center, and Center for Crop Genome Engineering, Longzi Lake Campus, Henan Agricultural University, Zhengzhou, China
- 2 State Key Laboratory of Plant Cell and Chromosome Engineering, Institute of Genetics and Developmental Biology, Chinese Academy of Sciences, Beijing, China
- 3 National Key Laboratory of Plant Molecular Genetics, CAS Center for Excellence in Molecular Plant Sciences, Shanghai Institute of Plant Physiology and Ecology, Shanghai Institutes for Biological Sciences, Chinese Academy of Sciences, Shanghai, China
- 4 University of the Chinese Academy of Sciences, Beijing, China
- 5 State Key Laboratory of Biology of Plant Diseases and Insect Pests, Institute of Plant Protection, Chinese Academy of Agricultural Sciences, Beijing, China
- 6 State Key Laboratory of Protein and Plant Gene Research, School of Life Sciences, Peking University, Beijing, China
- 7 National Biological Experimental Teaching Demonstration Center, College of Life Sciences, Henan Agricultural University, Zhengzhou, China
- 8 The Shennong Laboratory, Zhengzhou, China

\*Corresponding author. Tel: +86 10 64807609; E-mail: qhshen@genetics.ac.cn

\*\*Corresponding author. Tel: +86 13592581762; E-mail: mingyuegou@henau.edu.cn

\*\*\*Corresponding author. Tel: +86 371 56990317; E-mail: dwwang@henau.edu.cn

†These authors contributed equally to this work

by Dicer or Dicer-like proteins (Shen *et al.*, 2010; de Ronde *et al.*, 2013; Iki *et al.*, 2017; Zhang *et al.*, 2020; Han *et al.*, 2020a); the HC-Pro VSR of potyviruses binds vsiRNAs and prevents their loading into Argonaute (AGO) proteins (Lakatos *et al.*, 2006; Garcia-Ruiz *et al.*, 2015; Valli *et al.*, 2018); the 340R VSR of invertebrate iridescent virus 6 binds both dsRNAs and vsiRNAs and retards their processing and loading into AGOs (Bronkhorst *et al.*, 2019). However, it is still unclear if host may subvert VSRs or other viral pathogenic determinants to regulate viral proliferation in the infected cells.

Being the core components of RISC, AGOs have received considerable attention in the research on antiviral RNAi in plants (Fang & Qi, 2016; Guo *et al.*, 2019). The AGOs characterized to date all contain the conserved PIWI-ARGONAUTE-ZWILLE (PAZ), middle (MID), and PIWI domains (Fang & Qi, 2016); the PAZ domain enables AGOs to bind single-stranded nucleic acids; the MID domain specifically recognizes the 5' nucleotide of small RNAs (sRNAs); the PIWI domain has RNase H-like activity and allows AGOs to cleave the target RNAs bound by sRNAs. Recently, a study demonstrated that the P28 VSR of bamboo mosaic virus (BaMV) interacted with NbAGO10 and increased its accumulation in infected tobacco cells (Huang *et al.*, 2019). Additionally, NbAGO10 was found to associate with a small RNA-degrading nuclease 1 (NbSDN1), whose decreased expression by virus-induced gene silencing (VIGS) increased vsiRNA abundance and lowered BaMV RNA accumulation in tobacco cells. But it remains unknown if the P28 VSR may directly interact with NbSDN1 and whether the NbSDN1 involved may actually cleave vsiRNAs enzymatically.

SDNs and homologous proteins are widely present in plant and animal cells, with *Arabidopsis* SDN1 (AtSDN1) being demonstrated to cleave sRNAs through 3' trimming *in vivo*, which requires the interaction of SDN1 with the conserved PAZ domain of AGOs (Ramachandran & Chen, 2008; Yu *et al.*, 2017; Chen *et al.*, 2018). It has been proposed that the AGO-containing RISC can function in sRNA degradation or protection depending on whether there is SDN1 incorporation or not; this represents an important molecular mechanism for controlling sRNA homeostasis in cells (Ramachandran & Chen, 2008; Yu *et al.*, 2017; Chen *et al.*, 2018). Structural analysis has revealed that cleavage of sRNA by AtSDN1 is executed in the RISC; during the action of AtSDN1, its N-terminal domain binds and trims the 3' end of sRNA, while its C-terminal domain binds to target RNA to facilitate its enzymatic activity (Chen *et al.*, 2018). As demonstrated using recombinant protein, the cleavage products of AtSDN1 were approximately 8–9 nucleotides (nts) (Ramachandran & Chen, 2008). Considering that decreased SDN1 expression has been linked with elevated vsiRNA abundance of a plant virus (Huang *et al.*, 2019), the function of SDN1 in regulating vsiRNA homeostasis and the molecular mechanism involved merit deeper investigations.

Wheat, maize, and barley are among the most valuable food and feed crops in the world, but their production is constantly threatened by the epidemics of barley yellow dwarf viruses (BYDVs), a group of closely related luteoviruses carrying a positive-sense single-stranded RNA genome (Miller & Rasochová, 1997; Smirnova *et al.*, 2015; Ali *et al.*, 2018; Aradottir & Crespo-Herrera, 2021). Another group of RNA viruses, the cereal yellow dwarf viruses (CYDVs), also infect a wide range of cereal species, but they belong to poleroviruses (Ali *et al.*, 2018; Aradottir & Crespo-Herrera, 2021). Among the proteins encoded by BYDVs, the 17K protein (also named as P4) is an important virulence factor because it functions in viral movement, acts as

a VSR, and contributes strongly to host dwarfing through disrupting mitosis (Nass *et al.*, 1998; Fusaro *et al.*, 2017; Jin *et al.*, 2020). Furthermore, 17K is also conserved in diverse poleroviruses including CYDVs (Nass *et al.*, 1998; Ali *et al.*, 2018; Heck & Brault, 2018). Despite the importance of the BYDV 17K protein, the mode of action underlying its VSR activity remains unknown. Moreover, it is still unclear if the poleroviral 17K may also possess VSR activity. Therefore, further studies are necessary to understand the functions of luteoviral and poleroviral 17K proteins more deeply. This understanding may yield valuable strategies for controlling the diseases elicited by luteoviruses and poleroviruses.

Following on from previous studies on the multiple roles of 17K in BYDV pathogenesis (Nass *et al.*, 1998; Fusaro *et al.*, 2017; Jin *et al.*, 2020), we found here that the 17K protein of BYDV-GAV, a typical luteovirus and an important BYDV strain causing severe barley and wheat yellow dwarf disease (Jin *et al.*, 2004; Wang *et al.*, 2013), was phosphorylated by HvGRIK1-HvSnRK1 kinases in host cells, with the level of phosphorylated 17K (P17K hereafter) clearly increased by overexpressing HvSnRK1-YFP or markedly decreased by ectopically expressing HvSnRK1<sup>K139R</sup>-YFP (a dominant-negative mutant of HvSnRK1-YFP). Functional analysis showed that P17K, but not the unphosphorylated 17K, promoted anti-BYDV RNAi through elevating vsiRNA abundance. Mechanistic investigations revealed that 17K<sup>5D</sup>, a phosphomimic mutant of 17K, could bind barley small RNA-degrading nuclease 1 (HvSDN1) and BYDV vsiRNA, with both properties required for 17K<sup>5D</sup> to efficiently inhibit vsiRNA cleavage by recombinant HvSDN1. Notably, we detected the presence of vsiRNA-containing HvAGO1-P17K-HvSDN1 complex in BYDV-infected barley through analyzing the immunoprecipitates prepared using anti-HvAGO1 antibody; the activity of this complex in degrading vsiRNA was compromised in the host cells with more P17K, whereas the reverse was observed in those cells with less P17K. Moreover, P17K weakened the interaction between HvSDN1 and vsiRNA-carrying HvAGO1, thus hampering vsiRNA cleavage by HvSDN1. These data support the idea that host-mediated phosphorylation causes functional subversion of BYDV 17K, with the resulting P17K being able to enhance vsiRNA accumulation via inhibiting vsiRNA degradation by HvSDN1, which promotes anti-BYDV RNAi. Further supporting this novel antiviral RNAi-enhancing mechanism, we found that ectopic expression of 17K<sup>5D</sup> alone in wheat, or decreasing *SDN1* expression in barley by virus-induced gene silencing (VIGS) and in wheat by genome-editing, could significantly boost BYDV resistance in host plants via elevating vsiRNA abundance. Therefore, this newly discovered mechanism can be exploited to develop BYDV-resistant wheat and barley crops.

## Results

### 17K is phosphorylated in BYDV-infected barley plants

We examined the amino acid sequence of BYDV 17K and noted that two residues, T101 and S132, were located in two potential phosphorylation motifs of sucrose non-fermenting 1-related protein kinase 1 (SnRK1) (Fig EV1A), indicating that 17K might be phosphorylated by SnRK1. SnRK1 and its upstream kinase GRIK1 play a pivotal role in the response and adaptation of eukaryotes to biotic and abiotic stresses (Halford & Grahame Hardie, 1998; Emanuelle

et al, 2016; Hulsmans et al, 2016) and have been reported to phosphorylate plant viral proteins before (Shen & Hanley-Bowdoin, 2020). We thus monitored the phosphorylation status of BYDV 17K in infected barley plants using a Phos-tag SDS-PAGE-immunoblotting method (Kinoshita et al, 2016). Two sets of protein samples were prepared from viral-infected tissues at 0, 7, 14, and 21 days postinoculation (dpi), respectively. One set of samples were analyzed directly for detecting 17K phosphorylation, and the other set was treated with  $\lambda$ -protein phosphatase ( $\lambda$ -PP) and served as controls. As shown in Fig 1A, several phosphorylated bands of 17K, as well as the unphosphorylated 17K band, were found for the samples without  $\lambda$ -PP treatment, but the phosphorylated bands were not observed for the samples treated with  $\lambda$ -PP. This propelled us to examine the expression profiles of HvSnRK1 and its upstream kinase HvGRIK1 in BYDV-infected barley.

Compared with mock controls, the transcript levels of HvSnRK1 and HvGRIK1 were substantially higher in BYDV-infected plants, especially at 7 and 14 dpi (Fig EV1B and C). Consistently, the active form of HvSnRK1, detected with an antibody specific for a conserved and phosphorylated threonine residue in the T-loop of eukaryotic SnRK1 proteins (Shen et al, 2009; Shen & Hanley-Bowdoin, 2020), was largely elevated by BYDV infection, although the total amount of HvSnRK1, revealed using an antibody specific for eukaryotic SnRK1 proteins, did not change substantially in BYDV-infected plants and the mock controls (Fig 1B). These data suggest that BYDV 17K is phosphorylated in the host plants, likely by HvGRIK1-HvSnRK1 kinases.

### HvGRIK1-HvSnRK1 kinases interact with BYDV 17K and phosphorylate it *in vitro*

To test the phosphorylation of 17K by HvGRIK1-HvSnRK1 kinases, we first investigated whether 17K may bind HvGRIK1 and HvSnRK1 directly. Yeast two-hybrid (Y2H) assays showed that 17K physically interacted with HvGRIK1 and HvSnRK1 (Fig 1C and D). These interactions were subsequently verified by luciferase complementation (LC) experiments in *N. benthamiana* leaves (Fig EV1D and E). The interaction between 17K and HvSnRK1 was further validated using co-immunoprecipitation (Co-IP) assays (Fig EV1F), which was conducted with the transgenic barley plants ectopically expressing a 17K-GFP fusion protein (Jin et al, 2020).

To examine whether 17K, HvGRIK1, and HvSnRK1 may interact with each other *in planta*, we performed a dual-color trimolecular

fluorescence complementation experiment, which is highly efficient for analyzing the interactions among three proteins in plant cells (Offenborn et al, 2015). The result showed that 17K, HvGRIK1, and HvSnRK1 might interact with each other and formed a protein complex in *N. benthamiana* leaf cells (Fig EV1G).

Next, we conducted *in vitro* kinase assays to check the phosphorylation of 17K by HvGRIK1-HvSnRK1 kinases. 17K, HvGRIK1, and HvSnRK1 kinase domain (HvSnRK1-KD) were expressed in the bacterial cells and purified as N-terminal glutathione S-transferase (GST) fusion proteins. HvSnRK1-KD, but not full-length HvSnRK1, was used in the phosphorylation assays because intact recombinant HvSnRK1 tends to be insoluble and its kinase domain alone is sufficient for executing the kinase function *in vitro* (Shen et al, 2011; Han et al, 2020b). In Phos-tag SDS-PAGE coupled immunoblotting assays, multiple P17K bands were detected for the reactions containing GST-17K and GST-HvGRIK1 with or without the presence of GST-HvSnRK1-KD (Fig 1E, lanes 4 and 7). But the P17K bands were missing in the three control reactions (Fig 1E, lanes 1–3), which lacked GST-17K (lane 1), GST-HvGRIK1 and HvSnRK1-KD (lane 2), or GST-HvGRIK1 (lane 3). Notably, the P17K bands were more numerous in the reaction containing GST-17K, GST-HvSnRK1-KD, and GST-HvGRIK1 than in that with only GST-17K and GST-HvGRIK1 (Fig 1E, lane 7 vs. lane 4). These data indicate that GST-17K could be phosphorylated by GST-HvGRIK1 alone or by GST-HvGRIK1-activated GST-HvSnRK1-KD, with more extensive phosphorylation of 17K attained in the presence of both GST-HvGRIK1 and GST-HvSnRK1-KD.

To identify 17K residues phosphorylated in the *in vitro* kinase assays, the reaction products were digested by trypsin and analyzed using LC-MS/MS. Five residues of 17K, namely T101, T115, T128, S132, and T139, were phosphorylated in the reaction containing both GST-HvGRIK1 and GST-HvSnRK1-KD, whereas three 17K residues (T101, T128, and T139) underwent phosphorylation in the reaction with only GST-HvGRIK1 (Fig 1F, Appendix Fig S1 and Appendix Table S1). Apparently, T115 and S132 were phosphorylated in the reaction containing GST-HvGRIK1 and GST-HvSnRK1-KD but not in that with only GST-HvGRIK1, suggesting that phosphorylation of these two residues requires simultaneous presence of HvGRIK1 and HvSnRK1 (Fig. 1F, Appendix Fig S1 and Appendix Table S1). The finding that T101 and S132 were phosphorylated in the *in vitro* kinase assays is consistent with their location in the amino acid motifs likely recognized by SnRK1 (Fig EV1A).

#### Figure 1. Analysis of BYDV 17K protein phosphorylation *in vivo* and *in vitro*.

- A Detection of phosphorylated 17K in BYDV-infected cells using Phos-tag SDS-PAGE-immunoblotting assays with an anti-17K antibody. Dpi, days after BYDV inoculation; P, phosphorylated 17K bands;  $\lambda$ -PP,  $\lambda$ -phosphatase.
- B Active HvSnRK1, but not its total amount, was increased in BYDV-infected barley plants as compared with the mock controls. P-SnRK1 or SnRK1, enzymatically active SnRK1 (with T172 phosphorylation) or unphosphorylated SnRK1 protein.
- C, D Protein-protein interactions between 17K and HvGRIK1 (C) or HvSnRK1 (D) revealed using Y2H assays.
- E Analysis of 17K phosphorylation by HvGRIK1-HvSnRK1 kinases *in vitro*. The kinase reactions were set up by mixing the desired GST fusions of 17K, 17K<sup>3A</sup>, 17K<sup>5A</sup>, HvGRIK1, and HvSnRK1 kinase domain (KD), with the reaction products analyzed using Phos-tag SDS-PAGE-immunoblotting assays with an anti-17K antibody. P, phosphorylated 17K bands; arrowhead, unphosphorylated 17K.
- F A diagram showing BYDV 17K residues phosphorylated by HvGRIK1 alone or by HvGRIK1-HvSnRK1 cascade. The phosphorylated 17K residues were identified using LC-MS/MS experiment with higher than 91% of 17K amino acid covered in MS spectra.
- G Schematic representation of the dephosphomimic (17K<sup>3A</sup> and 17K<sup>5A</sup>) and phosphomimic (17K<sup>5D</sup>) mutants of BYDV 17K used in this study.

Data information: The datasets shown were reproducible in at least three independent experiments.

Source data are available online for this figure.

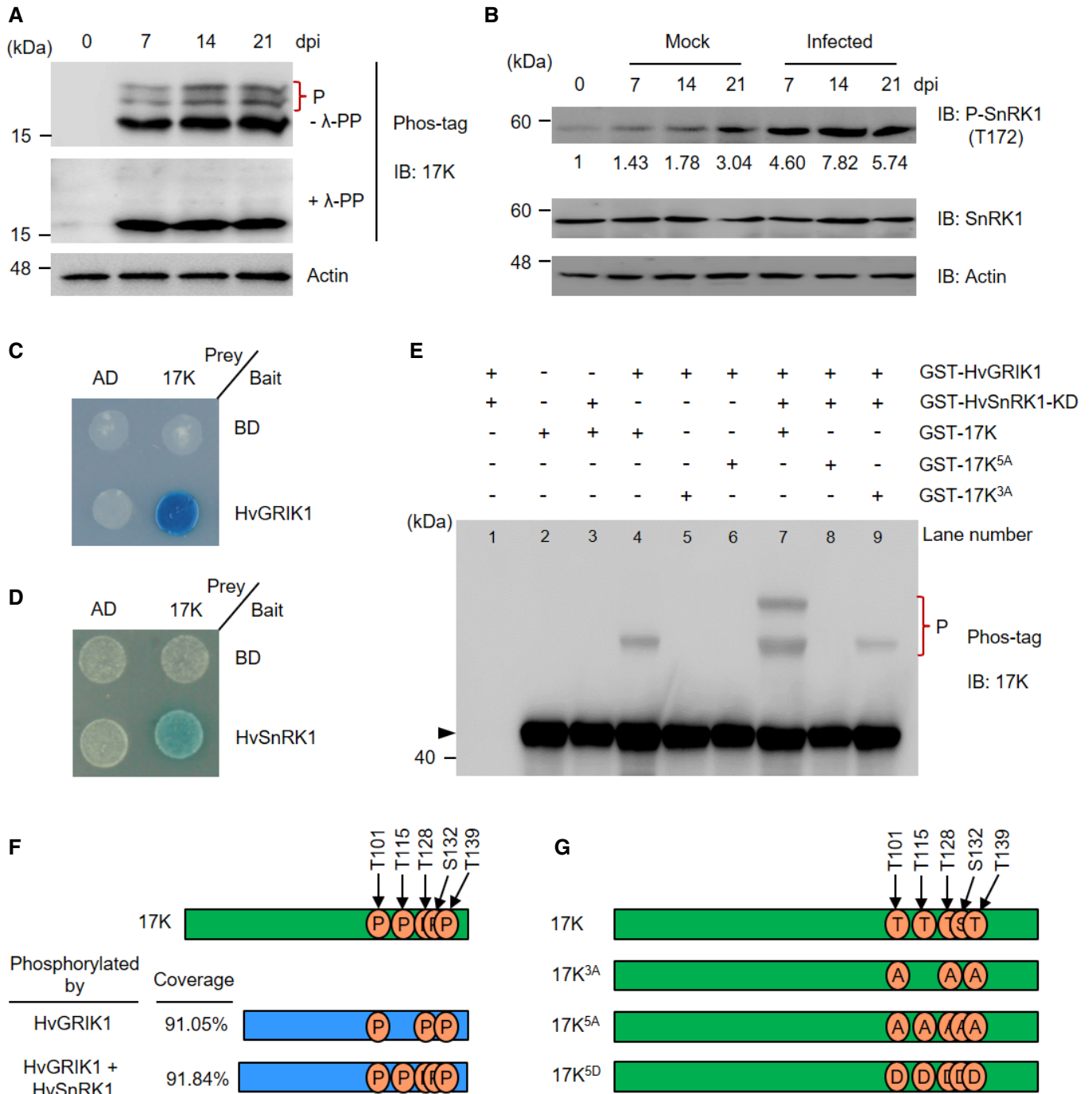


Figure 1.

Lastly, we generated two non-phosphorylated mutants of 17K, 17K<sup>3A</sup> (with T101, T128, and T139 all changed to alanine), and 17K<sup>5A</sup> (with T101, T115, T128, S132, and T139 all replaced by alanine) (Fig 1G), to verify the *in vitro* phosphorylation results presented above. No P17K bands were observed in the reaction in which GST-17K<sup>3A</sup> replaced the wild-type (WT) 17K in the presence of GST-HvGRIK1 (Fig 1E, lane 5), neither were P17K products detected in the assay that contained GST-17K<sup>5A</sup>, GST-HvGRIK1, and GST-HvSnRK1-KD (Fig 1E, lane 8). However, P17K products were detected for the reaction that contained 17K<sup>3A</sup> and both

GST-HvGRIK1 and GST-HvSnRK1-KD (Fig 1E, lane 9). This suggests that the two residues, T115 and S132, which were not mutated to alanine in 17K<sup>3A</sup> (Fig 1G), can be phosphorylated by GST-HvGRIK1-activated GST-HvSnRK1-KD, thus verifying the above suggestion that phosphorylation of T115 and S132 requires simultaneous presence of GST-HvGRIK1 and GST-HvSnRK1-KD. These *in vitro* assay data are consistent with the finding of P17K in BYDV-infected plants (Fig 1A) and suggest the phosphorylation of 17K residues by HvGRIK1-HvSnRK1 kinases (T101, T115, T128, S132, and T139) in host cells.

### Overexpression of HvSnRK1 enhances 17K phosphorylation and elevates antiviral defense via increasing vsiRNA abundance in natural BYDV infection

Based on the data presented above, we asked whether 17K could be phosphorylated in natural BYDV infection by HvSnRK1 and the consequences of 17K phosphorylation on host antiviral defense. To address these questions, we infected two type of transgenic barley plants, that is, SnRK1-YFP and SnRK1<sup>K139R</sup>-YFP, which overexpressed a YFP fused WT HvSnRK1 (HvSnRK1-YFP) or a dominant-negative mutant of HvSnRK1 (HvSnRK1<sup>K139R</sup>-YFP) (Cho *et al*, 2012; Han *et al*, 2020b), with BYDV. Immunoblotting assays confirmed the expression of HvSnRK1-YFP or HvSnRK1<sup>K139R</sup>-YFP each in two independent transgenic lines (Fig 2A). As revealed using Phos-tag SDS-PAGE coupled immunoblotting assays, the level of 17K phosphorylation was substantially higher in SnRK1-YFP-L4 than in SnRK1<sup>K139R</sup>-YFP-L13 or WT control (Fig 2B), indicating that HvSnRK1 indeed functions in 17K phosphorylation in BYDV-infected barley host cells.

Notably, the SnRK1-YFP transgenic plants were more resistant to BYDV infection than WT controls, because their BYDV symptoms (as indicated by reductions in plant height and root growth) were milder (Fig 2C–F); the proliferation of BYDV in SnRK1-YFP plants was also reduced, judging from significantly decreased expression of viral CP gene in them (Fig 2G and H). In contrast, SnRK1<sup>K139R</sup>-YFP plants were more susceptible to BYDV infection, because stronger BYDV symptoms and higher expression of viral CP gene were observed in SnRK1<sup>K139R</sup>-YFP individuals than in SnRK1-YFP or WT controls (Fig 2C–H). Enhancement of 17K phosphorylation by overexpressing HvSnRK1 therefore led to the upregulation of antiviral defense in BYDV-infected barley, which results in lowered viral proliferation and attenuated disease symptoms.

As 17K possesses VSR activity (Fusaro *et al*, 2017), we examined whether elevation of antiviral defense in SnRK1-YFP plants might be associated with increased abundance of BYDV vsiRNAs. We therefore conducted sRNA sequencing and comparatively analyzed vsiRNA accumulation levels in BYDV-infected SnRK1-YFP plants and WT controls at 4, 7, and 14 dpi. The abundance of vsiRNAs was significantly higher in SnRK1-YFP-L4 cells than in WT controls at all three time points, with the magnitude of vsiRNA upregulation in SnRK1-YFP-L4 being clearly stronger at 4 and 7 dpi (Fig 3A and B). This is consistent with the fact that antiviral RNA silencing mediated by vsiRNAs functions primarily at the early phase of viral infections

(Pertermann *et al*, 2018). The length of BYDV vsiRNAs varied from 21 to 24 nts, with the major type having 22 nts (Fig 3C), which agrees well with the previous findings made in analyzing vsiRNAs present in the plants infected by turnip yellows virus, cotton leaf roll dwarf virus, or BYDV-GAV (Silva *et al*, 2011; Shen *et al*, 2020; Clavel *et al*, 2021). The proportions of vsiRNAs with different sizes were similar in BYDV-infected SnRK1-YFP plants and WT controls (Fig 3C). This finding, together with the data depicted in Figs 1 and 2, suggests that phosphorylation of 17K by HvGRIK1-HvSnRK1 kinases promotes vsiRNA accumulation and antiviral defense in natural BYDV infection.

### 17K<sup>5D</sup> loses VSR activity and gains the ability to promote antiviral gene silencing

The experiments above led us to investigate the effect of phosphorylation of 17K on its VSR function. Hence, the VSR activities of 17K and two derivative mutants, 17K<sup>5A</sup> (a dephosphomimic mutant, see above) and 17K<sup>5D</sup> (a phosphomimic mutant with T101, T115, T128, S132, and T139 all changed to aspartic acid) (Fig 1G), were analyzed using the 16c tobacco line, which constitutively expressed a GFP transgene and highly useful for analyzing VSRs (Yaegashi *et al*, 2012). The P19 protein of tomato bushy stunt virus (TBSV), which debilitates gene silencing pathway by preventing efficient RISC assembly through binding siRNA duplexes (Vargason *et al*, 2003; Lakatos *et al*, 2004; Li & Wang, 2019), was used as a positive control for VSR activity. As anticipated, agroinfiltration of 35S::GFP in the absence of any VSR expression elicited transgene silencing and inhibited GFP fluorescence in 16c plants; the expression of P19 suppressed 35S::GFP-induced transgene silencing and resulted in clear GFP fluorescence in 16c leaves (Fig 4A). 17K and 17K<sup>5A</sup> behaved similarly in their suppression of 35S::GFP-induced gene silencing, but 17K<sup>5D</sup>, a mimic of phosphorylated 17K (P17K), exhibited little GFP silencing suppression activity (Fig 4A). Relative to the leaves without ectopic VSR expression, the abundance of GFP siRNAs was substantially reduced in the leaves with the expression of P19, 17K, or 17K<sup>5A</sup>, but was evidently increased in those with 17K<sup>5D</sup> expression (Fig 4B). Consistently, GFP transcripts were significantly more abundant in the leaves expressing P19, 17K, or 17K<sup>5A</sup>, but were much reduced in those with 17K<sup>5D</sup> expression (Fig EV2A). Using immunoblotting, we confirmed that GFP, 17K, 17K<sup>5A</sup>, and 17K<sup>5D</sup> were duly expressed in 16c leaves in the above experiment (Fig EV2B). Hence, phosphorylation of BYDV 17K, as revealed using

**Figure 2. Overexpression of HvSnRK1 increases 17K phosphorylation and promotes barley defense to BYDV.**

- A Confirmation of the expression of SnRK1<sup>K139R</sup>-YFP or SnRK1-YFP fusion protein each in two transgenic lines, SnRK1<sup>K139R</sup>-YFP-L13 and -L22 or SnRK1-YFP-L4 and -L17, by immunoblotting. The protein samples analyzed here or in (B) and (C) were all prepared from BYDV-infected barley plants at 21 dpi.
- B Phosphorylation of BYDV 17K was increased in SnRK1-YFP-L4 plants overexpressing SnRK1-YFP but reduced in SnRK1<sup>K139R</sup>-YFP-L13 ectopically expressing SnRK1<sup>K139R</sup>-YFP compared with WT control. P, phosphorylated 17K bands.
- C BYDV disease symptoms were substantially attenuated in the transgenic lines overexpressing SnRK1-YFP, but aggravated in those ectopically expressing SnRK1<sup>K139R</sup>-YFP compared with WT control.
- D–F Quantitative comparisons of plant height (D), maximum root length (E), and total root length (F) among the set of BYDV-infected barley materials shown in (C) (using the samples collected at 21 dpi).
- G, H Transcript (G) and protein (H) levels of viral CP gene in the set of BYDV-infected barley materials shown in (C) (using the samples collected at 21 dpi).

Data information: In (D–G), data are presented as means  $\pm$  SD of 30 (D–F) or 4 (G) plants for each line, with those labeled by different letters being significantly different.  $P < 0.001$  (D–F);  $P < 0.05$  (G), ANOVA and LSD for multiple comparisons. The datasets displayed in (A–C and H) were all representative of three independent experiments.

Source data are available online for this figure.

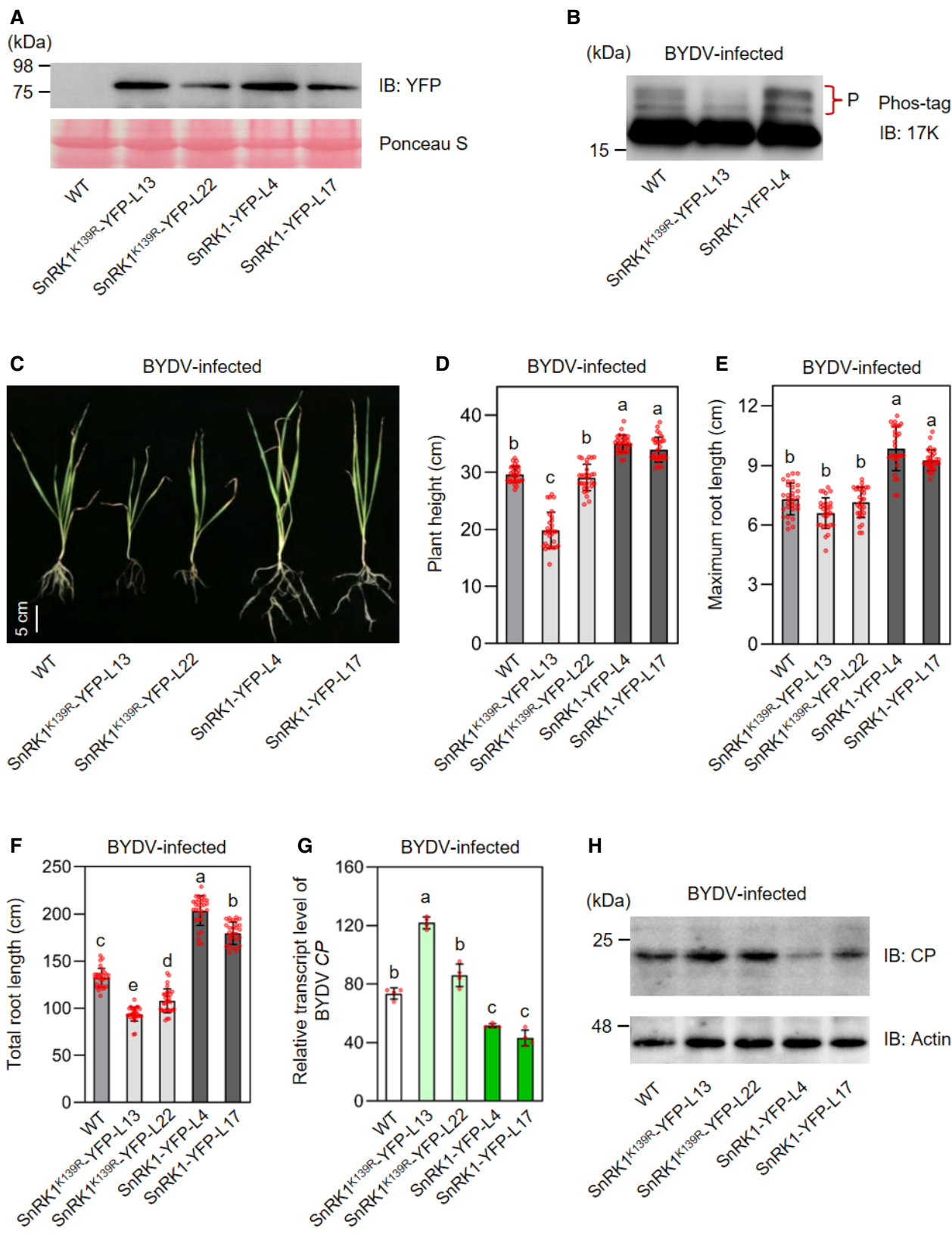
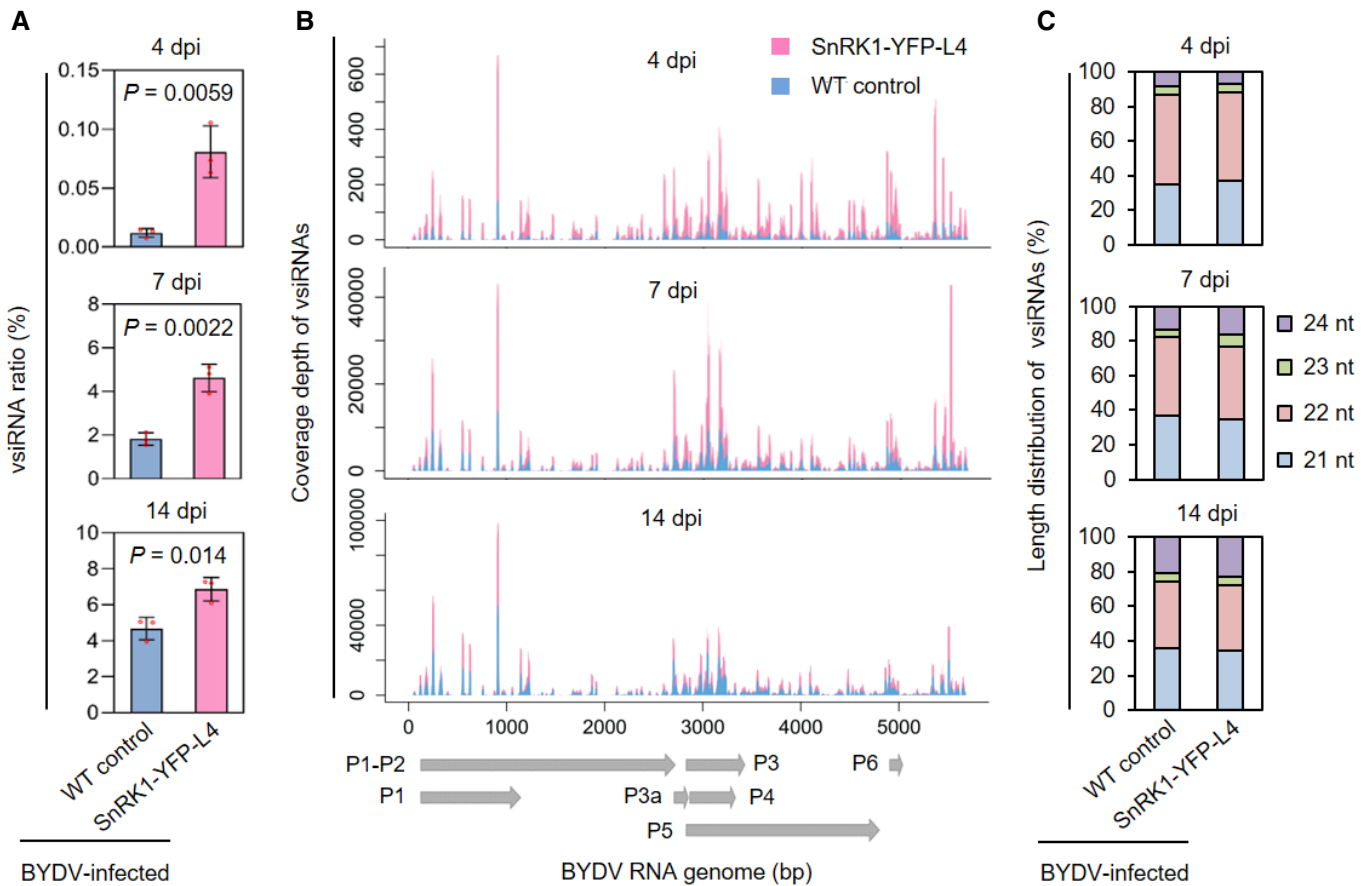


Figure 2.



**Figure 3. HvSnRK1 overexpression elevates BYDV vsRNA abundance.**

**A** BYDV vsRNA abundance, normalized and calculated as the ratio of total sRNAs sequenced, was significantly higher in the transgenic barley line SnRK1-YFP-L4 overexpressing SnRK1-YFP than in WT control at 4, 7, and 14 dpi.

**B** Coverage depth of vsRNAs along BYDV genomic RNA between viral-infected SnRK1-YFP-L4 and WT control plants at 4, 7, and 14 dpi. The seven BYDV genes (shaded gray) are provided below the graph.

**C** Comparison of the percentages of 21–24 nt BYDV vsRNAs between BYDV-infected SnRK1-YFP-L4 and WT control plants at 4, 7, and 14 dpi.

Data information: In (A), data are presented as means  $\pm$  SD ( $n = 3$  biological repeats), with the  $P$ -values calculated using Student's  $t$ -test. In (B), Coverage depth was calculated using the data from three biological repeats. In (C), each percentage was calculated using the data from three biological repeats.

Source data are available online for this figure.

17K<sup>5D</sup>, inhibits its VSR activity. The fact that 17K<sup>5D</sup> expression promoted GFP siRNA accumulation in 16c leaves (Fig 4B) points to the possibility that P17K may actually enhance gene silencing via elevating siRNA abundance.

We then examined whether 17K and 17K<sup>5D</sup> may differ in their ability to regulate vsRNA accumulation in virus-infected cells. Because a full-length infectious clone that can efficiently infect barley and wheat is not yet available for BYDV, we introduced the coding sequence of 17K, 17K<sup>5A</sup>, or 17K<sup>5D</sup> into the genome of pea early browning virus (PEBV), which is a bipartite RNA virus with its full-length infectious clones capable of infecting tobacco (Constantin *et al.*, 2004). PEBV-GFP (expressing free GFP) and three more recombinant viruses (PEBV-17K, PEBV-17K<sup>5A</sup>, and PEBV-17K<sup>5D</sup>) were each introduced into tobacco plants, with viral accumulation determined by measuring the transcript levels of two PEBV genes, the 30K gene located on RNA1 and the coat protein gene CP on RNA2 (Fig 4C). Compared with the infection by PEBV-GFP, viral

proliferation in the plants infected by PEBV-17K or PEBV-17K<sup>5A</sup> was strongly enhanced, but in PEBV-17K<sup>5D</sup>-infected tobacco cells, PEBV amplification was significantly decreased (Figs 4D and EV2C). Consistently, PEBV CP accumulated to much higher levels in PEBV-17K or PEBV-17K<sup>5A</sup>-infected tissues relative to those infected by PEBV-GFP or PEBV-17K<sup>5D</sup> (Fig 4E).

The vsRNAs in the plants infected by PEBV-GFP, PEBV-17K, or PEBV-17K<sup>5D</sup> were investigated using sRNA sequencing. Here, we focused on vsRNAs derived from only the RNA1 of PEBV genome, as the RNA2 was modified and differed among the three recombinant PEBVs used in this experiment (Fig 4C). Compared with PEBV-GFP-infected plants, the level of RNA1-derived vsRNAs was significantly decreased in those infected by PEBV-17K (Figs 4F and EV2D), which is consistent with the conspicuous VSR activity of 17K (Fig 4A). In contrast, the abundance of RNA1-derived vsRNAs in PEBV-17K<sup>5D</sup>-infected plants was markedly higher than that determined for the individuals infected by PEBV-GFP (Figs 4F and

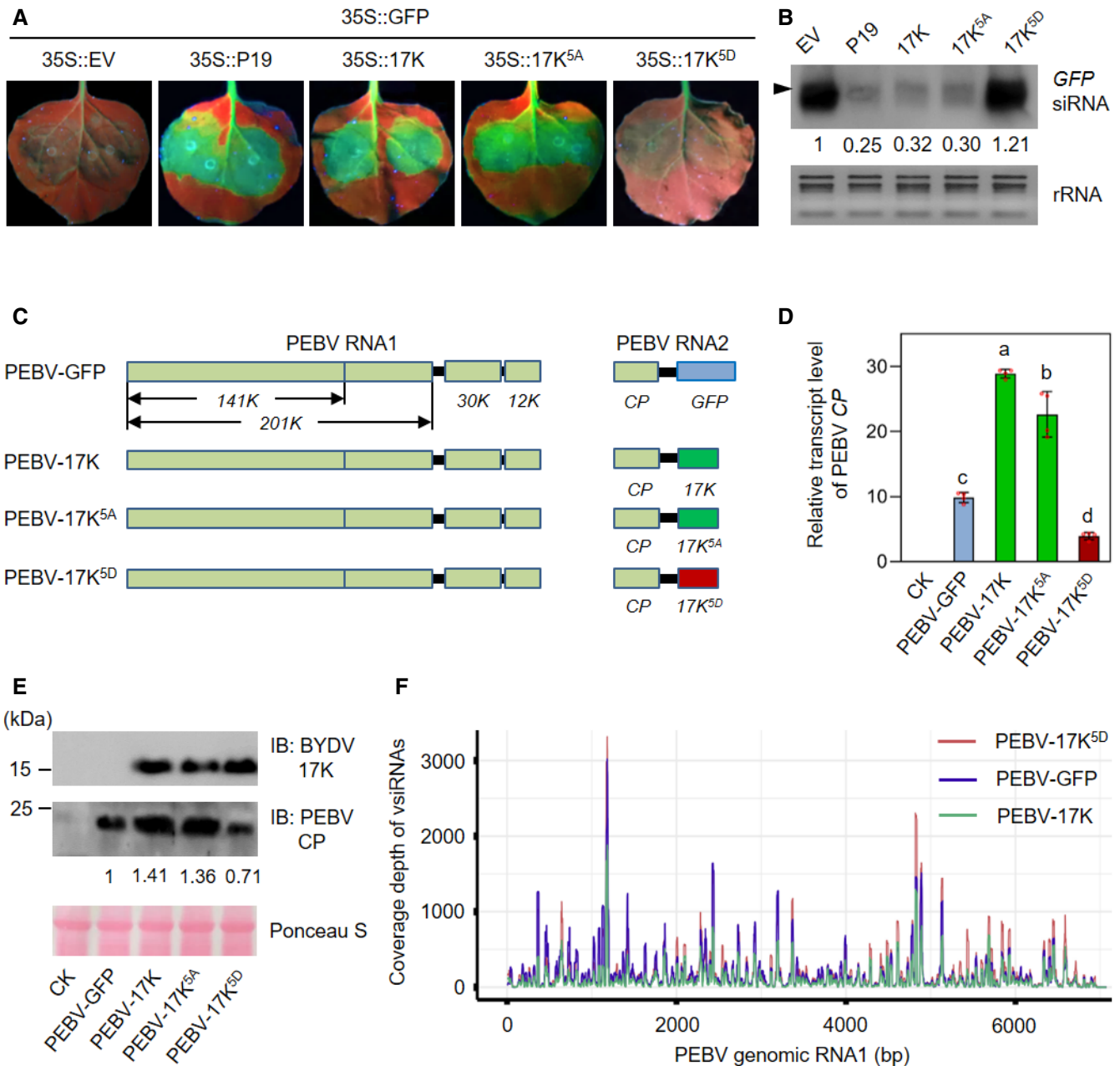


**Figure 4. Effects of phosphorylation on the VSR activity of BYDV 17K as analyzed using phosphomimic (17K<sup>5D</sup>) and dephosphomimic (17K<sup>5A</sup>) mutants.**

**A** The VSR function of 17K<sup>5D</sup> was drastically decreased compared to 17K and 17K<sup>5A</sup>, as assessed using the 16c transgenic tobacco. The P19 VSR of tomato bushy stunt virus and an empty plasmid vector (35S::EV) were used as positive and negative controls, respectively. The GFP fluorescence was imaged at 4-day post agroinfiltration of the indicated constructs.

**B** Levels of GFP siRNA detected by sRNA blotting for the panel of tobacco materials shown in (A), with arrowhead indicating the main band of GFP siRNA.

**C** A diagram illustrating four recombinant pea early browning virus (PEBV) vectors, with the RNA2 modified to express GFP, 17K, 17K<sup>5A</sup>, or 17K<sup>5D</sup>. The original RNA2 genes, 29.8K and 23K (Goulden *et al*, 1990; Constantin *et al*, 2004), were replaced by the coding sequence of GFP, 17K, 17K<sup>5A</sup>, or 17K<sup>5D</sup> in the recombinant viruses shown. The five PEBV genes, including 30K on RNA1 and CP on RNA2 are depicted.

**D** Transcript levels of CP in the tobacco plants infected by four recombinant PEBVs at 21 dpi. CK, uninfected plants.

**E** Protein levels of PEBV CP and corrected expression of 17K, 17K<sup>5A</sup>, or 17K<sup>5D</sup> in the panel of tobacco plants shown in (D), revealed using immunoblotting with anti-PEBV CP or anti-17K antibody.

**F** Coverage depth of vsRNAs along PEBV genomic RNA1 obtained for the plants infected by PEBV-17K<sup>5D</sup>, PEBV-GFP, or PEBV-17K. sRNA sequencing was conducted at 14 dpi with three biological repeats.

Data information: In (D), data are means  $\pm$  SD ( $n = 4$  biological replicates), with those labeled by different letters being significantly different ( $P < 0.05$ , ANOVA and LSD for multiple comparisons). The datasets displayed in (A, B, and E) were typical of three independent experiments.

Source data are available online for this figure.

EV2D), which is in agreement with the promotion of GFP siRNAs by 17K<sup>5D</sup> in 16c tobacco (Fig 4B). The size of PEBV vsRNAs was mainly 21–24 nts, with those having 21 or 22 nts being the major types in the plants infected by PEBV, PEBV-17K, or PEBV-17K<sup>5D</sup> (Fig EV2E). Thus, compared with 17K, its phosphomimic mutant, 17K<sup>5D</sup> is deficient in VSR activity and acquires the ability to upregulate antiviral gene silencing through enhancing vsRNA abundance in viral-infected plants.

### 17K<sup>5D</sup> differs from 17K in interacting with HvSDN1 and binding to single-stranded vsRNA

To obtain insight into the molecular mechanism underlying the enhancement of vsRNA abundance and antiviral RNAi by P17K (Figs 2 and 3) and 17K<sup>5D</sup> (Fig 4), we investigated whether 17K<sup>5D</sup> and 17K may vary in their ability to interact with SDN proteins, which have recently been found to degrade sRNAs through 3' end trimming (Ramachandran & Chen, 2008; Yu et al, 2017; Chen et al, 2018). Two *HvSDN* genes, *HvSDN1* and *HvSDN5*, phylogenetically related to *Arabidopsis AtSDN1* (*At3g50100*) and *AtSDN5* (*At5g25800*), respectively (Appendix Fig S2), were identified by searching barley genome sequence. We selected *HvSDN1* as a representative for this study because of its close phylogenetic relatedness with *AtSDN1*. In Y2H and LC assays, we found that 17K<sup>5D</sup>, but not 17K, consistently interacted with *HvSDN1* in yeast and tobacco cells (Fig 5A and B). Judging from the qRT-PCR and immunoblotting data presented in Appendix Fig S3, *HvSDN1* was actively expressed in barley plants although its transcript and protein levels were not substantially altered by BYDV infection.

We next tested whether 17K<sup>5D</sup> and 17K may differ in vsRNA binding by performing RNA electrophoretic mobility shift assays (EMSAs) using vsRNA899, a highly abundant single-stranded 21 nt vsRNA derived from BYDV RNA genome (899–919 bp) in BYDV-infected barley (Fig 3B), as a probe. In repeated RNA EMSAs, 17K<sup>5D</sup>, but not 17K, was found to bind vsRNA899, but neither 17K nor 17K<sup>5D</sup> showed binding to vsRNA899 duplex (Fig 5C). Collectively, these data indicate that 17K<sup>5D</sup> is distinct from 17K; in that, it is able to interact with *HvSDN1* and to bind BYDV vsRNA.

### 17K<sup>5D</sup> inhibits *HvSDN1*-catalyzed cleavage of BYDV vsRNA *in vitro*

The higher levels of P17K and vsRNAs in BYDV-infected ShRK1-YFP-L4 plants (Figs 2 and 3), together with the findings that 17K<sup>5D</sup>, but not 17K, interacted with *HvSDN1* and vsRNAs (Fig 5), urged us to examine whether 17K<sup>5D</sup> may inhibit *HvSDN1*-catalyzed vsRNA cleavage. To facilitate this examination, we developed a non-radioactive and convenient *in vitro* sRNA (vsRNA) cleavage assay by recombinant SDN1, which involved labeling vsRNA 5' end by a biotin moiety, with the cleavage products detected by enhanced chemiluminescence. Using this method and with BYDV vsRNA899 as a substrate, we found that recombinant *HvSDN1*, as well as *AtSDN1*, cleaved vsRNAs based on the production of smaller RNA fragments of 8–9 nts, but neither 17K<sup>5D</sup> nor 17K showed this activity (Fig 6A). Furthermore, we observed that *HvSDN1*-catalyzed vsRNA899 cleavage was clearly inhibited by increasing amounts of GST-17K<sup>5D</sup> but not by GST-17K (Fig 6B).

Considering that 17K<sup>5D</sup> had been found to bind BYDV vsRNAs (Fig 5C), we analyzed whether this binding may contribute to the inhibition of *HvSDN1*-catalyzed vsRNA cleavage by 17K<sup>5D</sup>. We thus developed three mutants of 17K<sup>5D</sup> (17K<sup>5D</sup>m4, 17K<sup>5D</sup>m2a, and 17K<sup>5D</sup>m2b, Fig 6C) by mutating the four arginine residues (R144, R148, R152, and R154) located at the C-terminus of 17K, which have been shown involved in the RNA binding activity of recombinant 17K (Xia et al, 2008). In 17K<sup>5D</sup>m4, the four arginine (R) residues were all changed to glutamic acid (E), with R148 and R152 replaced by E in 17K<sup>5D</sup>m2a and R148 and R154 by E in 17K<sup>5D</sup>m2b (Fig 6C). The three mutants all interacted with *HvSDN1* similarly as 17K<sup>5D</sup> (Figs 6C and EV3A), but their GST fusions failed to bind vsRNA899 contrary to GST-17K<sup>5D</sup> in RNA EMSAs (Fig 6D).

To compare whether 17K<sup>5D</sup> and three derivative mutants (i.e., 17K<sup>5D</sup>m4, 17K<sup>5D</sup>m2a, and 17K<sup>5D</sup>m2b) may differ in the inhibition of vsRNA cleavage by *HvSDN1* in a quantitative manner, we innovated a fluorescent *in vitro* sRNA (vsRNA) cleavage assay, with the vsRNA substrate (vsRNA899) prepared by labeling the 5' end with carboxyfluorescein and the 3' end with carboxytetramethylrhodamine. When the vsRNA is intact, the fluorescence emitted by carboxyfluorescein is quenched by the closely spaced carboxytetramethylrhodamine; 3' end trimming by SDN1 would separate away carboxytetramethylrhodamine, thus allowing fluorescence to be recorded by appropriate fluorescent detectors (Fig 6E). In agreement with this design, we found that the fluorogenic vsRNA899 substrate was cleaved by *HvSDN1* in the assays containing GST or GST-17K, with strong fluorescence readily detected by Typhoon FLA 9500 (Fig 6F and G). However, in the assays supplemented with 17K<sup>5D</sup>, 17K<sup>5D</sup>m4, 17K<sup>5D</sup>m2a, or 17K<sup>5D</sup>m2b, *HvSDN1*-catalyzed vsRNA cleavage was significantly decreased by 28.84–53.46%, with the scale of the decrease being significantly larger in the presence of 17K<sup>5D</sup> (53.46%) relative to that of 17K<sup>5D</sup>m4, 17K<sup>5D</sup>m2a, or 17K<sup>5D</sup>m2b (28.84–34.60%) (Fig 6G). In further assays, we established a standard curve between the amounts of vsRNA cleaved and the fluorescence yields recorded using Roche LC 480 (Fig EV3B and C). Based on this curve, we estimated that, in a 30-min reaction time, approximately 1.53–1.57  $\mu$ M of vsRNA899 were cleaved by *HvSDN1* in the presence of GST or GST-17K, but the amounts of vsRNA899 cleaved dropped to 0.85–1.24  $\mu$ M when 17K<sup>5D</sup>, 17K<sup>5D</sup>m4, 17K<sup>5D</sup>m2a, or 17K<sup>5D</sup>m2b were added to the assays (Fig 6H).

The above results suggest that recombinant *HvSDN1* cleaves BYDV vsRNA, which is inhibited by 17K<sup>5D</sup> but not by 17K. Because *HvSDN1* cleavage of vsRNA899 was more strongly inhibited by 17K<sup>5D</sup> than by its three derivative mutants (Fig 6F–H), the abilities of 17K<sup>5D</sup> to interact with *HvSDN1* and to bind vsRNA both contribute to its inhibition of *HvSDN1*-catalyzed vsRNA cleavage. Consistent with this proposition, we observed that the three derivative mutants were not as effective as 17K<sup>5D</sup> in suppressing GFP fluorescence in 16c tobacco plants (Appendix Fig S4). Based on this result, we deduce that these mutants may not be as competent as 17K<sup>5D</sup> in inhibiting *HvSDN1* cleavage of BYDV vsRNAs in host cells owing to losing RNA binding activity.

### P17K impedes the degradation of HvAGO1-associated vsRNAs by *HvSDN1* in BYDV-infected barley

As 17K<sup>5D</sup> inhibited vsRNA cleavage by recombinant *HvSDN1*, it became necessary to examine whether P17K may disrupt the

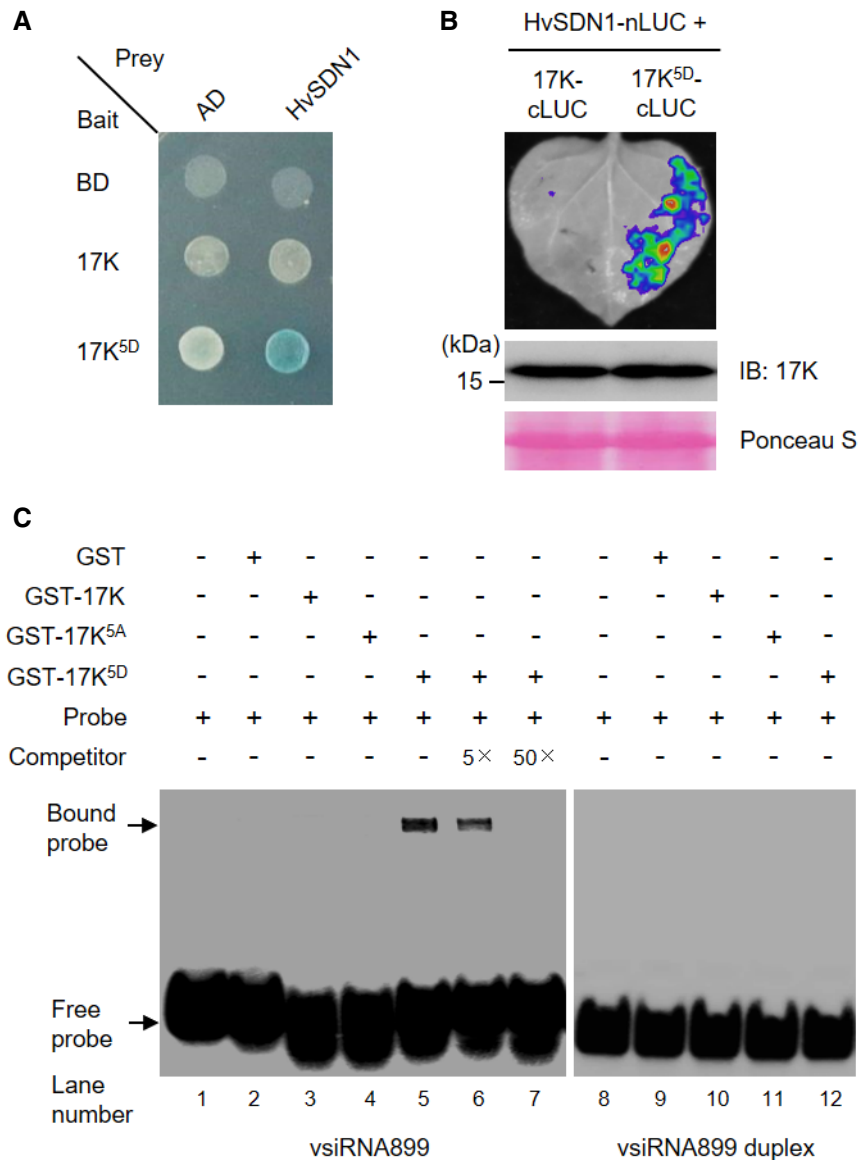


**Figure 5. 17K<sup>5D</sup> interacts with HvSDN1 and binds BYDV vsRNA.**

A, B 17K<sup>5D</sup>, but not BYDV 17K, interacted with HvSDN1 in Y2H (A) and LC (B) assays. Expression of 17K and 17K<sup>5D</sup> in the LC assays was verified by immunoblotting using anti-17K antibody.

C 17K<sup>5D</sup>, but not 17K or 17K<sup>5A</sup>, showed binding to BYDV vsRNA. The GST fusions of 17K, 17K<sup>5D</sup>, and 17K<sup>5A</sup>, as well as free GST, were used in the RNA EMSA assays with biotin-labeled vsRNA899 or vsRNA899 duplex as probes.

Data information: The experiments shown were all repeated three times with similar results obtained.

Source data are available online for this figure.

degradation of BYDV vsRNAs by HvSDN1 in the host cells. Considering the observation that sRNA cleavage by AtSDN1 is executed in the RISC (Chen *et al*, 2018) and our result that 17K<sup>5D</sup> interacted with HvSDN1, we hypothesized that HvSDN1 could degrade the vsRNAs associated with HvAGO1 by binding to HvAGO1 and that P17K could impede this degradation process by binding to HvAGO1 and HvSDN1. To test this hypothesis, we first investigated whether 17K<sup>5D</sup> (mimicking P17K) may interact with HvAGO1 and whether HvSDN1 may bind HvAGO1 *in vitro*. Y2H assays showed that 17K<sup>5D</sup>, as well as the unphosphorylated 17K, interacted with

HvAGO1, with the PAZ and PIWI domains of HvAGO1 directly involved in the interaction (Fig 7A). These interactions were subsequently validated using LC assays in tobacco leaves (Fig EV4A and B). Likewise, HvSDN1 was found to interact with HvAGO1 in both Y2H and LC assays (Figs 7A and EV4C).

Following the above results, we analyzed whether P17K may form a complex with HvSDN1 and vsRNA-containing HvAGO1 in BYDV-infected host cells. To this end, we prepared polyclonal antibodies to HvAGO1 or HvSDN1 (Fig EV4D and E), and conducted Co-IP assays with the input samples collected from BYDV-infected

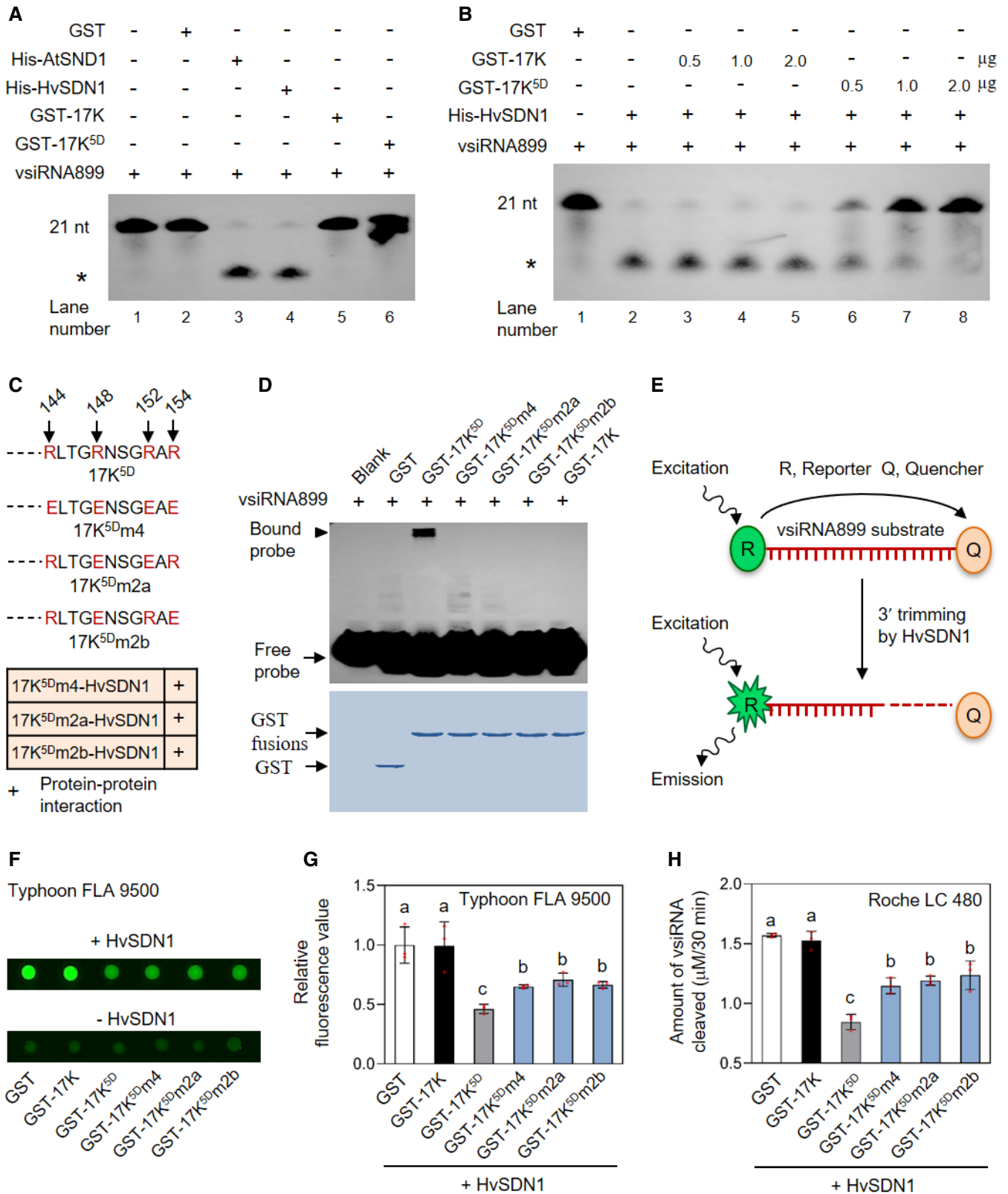


Figure 6.

**Figure 6. 17K<sup>5D</sup> impairs vsiRNA cleavage by recombinant HvSDN1 *in vitro*.**

- A Cleavage of BYDV vsiRNA899 by HvSDN1 (His-HvSDN1), with AtSDN1 (His-AtSDN1) serving as a positive control. Asterisk denotes cleavage products. The GST fusions of 17K and 17K<sup>5D</sup> did not show vsiRNA cleavage activity.
- B Inhibition of HvSDN1-catalyzed vsiRNA cleavage by GST-17K<sup>5D</sup> but not GST-17K. Free GST protein served as a negative control. Asterisk denotes cleavage products.
- C, D The three mutants of 17K<sup>5D</sup> (17K<sup>5D</sup>m4, 17K<sup>5D</sup>m2a, and 17K<sup>5D</sup>m2b) retained the ability to interact with HvSDN1 as revealed using LC assays (C), but their GST fusions failed to bind vsiRNA899 (D). Neither GST nor GST-17K showed vsiRNA899 binding.
- E A fluorogenic substrate for quantitatively analyzing the enzymatic activity of HvSDN1. The 5' and 3' ends of vsiRNA899 were labeled by 5-carboxyfluorescein (R) and carboxytetramethylrhodamine (Q), respectively. Cleavage of such labeled vsiRNA substrate by HvSDN1 would remove the quenching activity of Q, thus allowing the emitted fluorescence to be recorded by suitable detectors.
- F–H Quantitative analysis of HvSDN1 cleavage activities, with the fluorescence recorded using Typhoon FLA9500 (F and G) or Roche LC 480 platform (H). Compared with free GST or GST-17K, the GST fusions of 17K<sup>5D</sup> or three derivative mutants (17K<sup>5D</sup>m4, 17K<sup>5D</sup>m2a, and 17K<sup>5D</sup>m2b) inhibited HvSDN1-catalyzed cleavage of fluorogenic vsiRNA899, which was revealed by a fluorospot assay (F), relative comparison of fluorescence values (G), or comparison of the absolute amounts of vsiRNA cleaved by HvSDN1 (H).

Data information: In (G and H), data are means  $\pm$  SD ( $n = 3$  independent assays), with those labeled by different letters being significantly different ( $P < 0.05$ , ANOVA and LSD for multiple comparisons). The datasets displayed in (A, B, and D) were reproducible in three separate experiments.

Source data are available online for this figure.

WT barley, SnRK1<sup>K139R</sup>-YFP-L13, and SnRK1-YFP-L4 plants, respectively. The latter two types of plants overexpressed a dominant-negative mutant of HvSnRK1 or a functional HvSnRK1 protein, with SnRK1-YFP-L4 individuals exhibiting higher accumulation of P17K, elevated vsiRNA abundance, and enhanced BYDV resistance (Figs 2 and 3).

In the immunoprecipitates prepared using the HvAGO1 antibody, both P17K and HvSDN1 were detected (Fig 7B). As shown by Phos-tag SDS-PAGE coupled immunoblotting assays, a considerably higher amount of P17K was found for SnRK1-YFP-L4 than for WT and SnRK1<sup>K139R</sup>-YFP-L13 plants. However, much less HvSDN1 was detected for SnRK1-YFP-L4 than for WT and SnRK1<sup>K139R</sup>-YFP-L13 samples (Fig 7B). Compared with WT controls, the level of BYDV vsiRNAs in the immunoprecipitates was evidently higher for SnRK1-YFP-L4 plants but much lower for SnRK1<sup>K139R</sup>-YFP-L13 individuals (Fig 7B). Unphosphorylated 17K was also detected in HvAGO1 immunoprecipitates (Fig 7B), consistent with the finding that 17K showed interaction with HvAGO1 (Figs 7A and EV4B). The data depicted in Fig 7A and B suggest the formation of a vsiRNA-containing HvAGO1-HvSDN1-P17K complex in BYDV-infected host cells. Because a higher amount of P17K correlated with more abundant vsiRNAs in HvAGO1 immunoprecipitates (as found for BYDV-infected SnRK1-YFP-L4 plants), it is very likely that P17K impedes the degradation of HvAGO1-associated vsiRNAs by HvSDN1. This is further supported by decreased vsiRNA abundance in the HvAGO1 immunoprecipitates of BYDV-infected SnRK1<sup>K139R</sup>-YFP-L13 plants that contained much less P17K.

The observation that more P17K but less HvSDN1 were detected in the HvAGO1 immunoprecipitates of BYDV-infected SnRK1-YFP-L4 plants led us to test whether the interaction between HvAGO1 and HvSDN1 may be negatively affected by P17K. We thus compared the levels of HvAGO1 associated with HvSDN1 in BYDV-infected WT control, SnRK1<sup>K139R</sup>-YFP-L13, and SnRK1-YFP-L4 plants. In the immunoprecipitates prepared using anti-HvSDN1 antibody, the level of HvAGO1 detected was lowest for SnRK1-YFP-L4 plants but highest for SnRK1<sup>K139R</sup>-YFP-L13 individuals (Fig 7C). Consistent with this result, we observed that the interaction between HvAGO1 PAZ domain and HvSDN1 was significantly compromised in the presence of 17K<sup>5D</sup> (representing P17K) compared with the expression of unphosphorylated 17K in tobacco leaf cells (Fig 7D). These two lines of evidence indicate that P17K weakens the interaction between HvAGO1 and HvSDN1 in BYDV-infected plants.

From the datasets described above, it is apparent that the accumulation of P17K due to HvGRIK1-HvSnRK1-mediated phosphorylation leads to the formation of a vsiRNA-containing HvAGO1-P17K-HvSDN1 complex, which decreases the cleavage of HvAGO1-carried vsiRNAs by HvSDN1, thus elevating vsiRNA abundance and anti-BYDV RNAi in BYDV-infected barley. We therefore conclude that P17K and HvSDN1 are crucial for the ability of this complex to affect BYDV vsiRNA abundance.

### Transgenic expression of 17K<sup>5D</sup> in wheat promotes anti-BYDV RNAi

The above proposition urged us to seek genetic evidence for the enhancement of anti-BYDV RNAi by P17K. Therefore, we ectopically expressed 17K<sup>5D</sup> (mimicking P17K) in hexaploid common wheat, which is a widely cultivated staple food crop frequently damaged by BYDV epidemics (Miller & Rasochová, 1997; Ali *et al*, 2018; Aradottir & Crespo-Herrera, 2021). Two independent transgenic lines (17K<sup>5D</sup>-L3 and 17K<sup>5D</sup>-L7), expressing 17K<sup>5D</sup> as detected by immunoblotting (Fig 8A), were analyzed. The expression of 17K<sup>5D</sup> did not appear to affect the growth and development of common wheat (Appendix Fig S5). However, 17K<sup>5D</sup>-L3 and 17K<sup>5D</sup>-L7 were significantly more resistant to BYDV infection than WT control, as both transgenic lines showed improved plant growth (Fig 8B and C) and longer maximum root length (Fig 8D) at 21 dpi. The proliferation of BYDV in 17K<sup>5D</sup> transgenic plants was largely decreased compared with that observed for WT controls based on assessing the transcript and protein levels of viral CP gene (Fig 8E and F). BYDV vsiRNA abundance was substantially higher in the 17K<sup>5D</sup> transgenic plants than in WT controls at 14 dpi (Fig 8G). These data suggest that transgenic expression of 17K<sup>5D</sup> can increase BYDV defense accompanied by increased vsiRNA abundance, thus providing genetic evidence for P17K to promote anti-BYDV RNAi.

### Manipulating SDN1 expression *in planta* alters virus proliferation through changing vsiRNA abundance

We manipulated the expression level of *SDN1* in plant cells to obtain genetic evidence for its function in antiviral RNAi. First, the expression of *HvSDN1* in barley plants was silenced using VIGS with the viral vector derived from barley stripe mosaic virus (BSMV) (Yuan

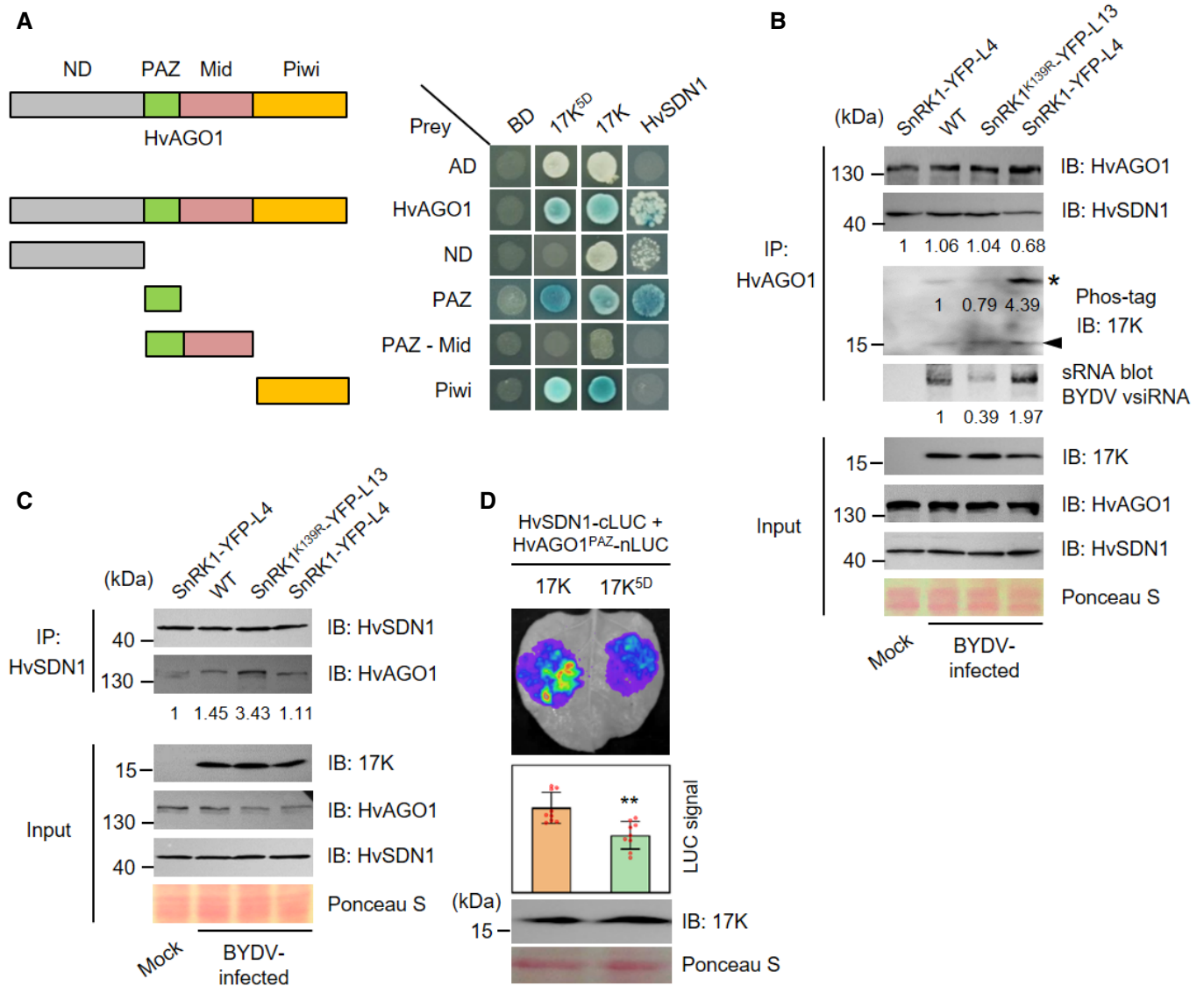


**Figure 7. P17K impedes the degradation of HvAGO1-associated vsiRNA by HvSDN1 in BYDV-infected barley.**

- A** Protein–protein interactions detected for 17K<sup>5D</sup> and HvAGO1, 17K and HvAGO1, or HvSDN1 and HvAGO1 using Y2H assays. Both 17K<sup>5D</sup> and 17K interacted with HvAGO1 through binding to its PAZ and Piwi domains. HvSDN1 interacted with HvAGO1 through the PAZ domain.
- B** Co-IP assays revealing the presence of vsiRNA-containing HvAGO1–HvSDN1–P17K complex in BYDV-infected WT, SnRK1<sup>K139R</sup>-YFP-L13, and SnRK1-YFP-L4 plants, with mock-inoculated SnRK1-YFP-L4 individuals as controls. The immunoprecipitates, prepared using anti-HvAGO1 antibody, were analyzed for the presence of HvSDN1 (by immunoblotting with anti-HvSDN1 antibody), P17K (asterisk) and 17K (arrowhead) (using Phos-tag SDS–PAGE coupled immunoblotting), and BYDV vsiRNA (by sRNA blotting). Compared with WT control, the HvAGO1 immunoprecipitates derived from SnRK1-YFP-L4 contained higher levels of P17K and vsiRNA but less amount of HvSDN1, whereas the reverse was observed for SnRK1<sup>K139R</sup>-YFP-L13.
- C** Co-IP assays demonstrating that the interaction between HvAGO1 and HvSDN1 was weakened by P17K. The immunoprecipitates were prepared using anti-HvSDN1 antibody from the panel of plants shown in (B). Relative to WT control, the HvSDN1 immunoprecipitates derived from SnRK1-YFP-L4 contained much less HvAGO1, whereas the opposite was observed for SnRK1<sup>K139R</sup>-YFP-L13.
- D** 17K<sup>5D</sup> compromised the interaction between HvSDN1 and the PAZ domain of HvAGO1. The LUC signal resulted from the interaction between HvSDN1–HvAGO1 PAZ domain was significantly decreased in the presence of 17K<sup>5D</sup> but not that of 17K.

Data information: In (B and C), the relative band intensities were obtained using ImageJ software. In (D), data are means  $\pm$  SD ( $n = 9$  biological replicates). \*\* $P < 0.01$  (Student's  $t$ -test). The datasets shown in (A–C) were all representative of three independent assays. Source data are available online for this figure.

et al., 2011). Compared with the controls inoculated with the empty BSMV vector (BSMV-EV), *HvSDN1* transcript level was significantly reduced in the barley plants infected by BSMV-SDN1gs designed

specifically to silence *HvSDN1* (Fig EV5A). The plants infected by BSMV-EV or BSMV-SDN1gs were further treated with virus-free or BYDV-carrying aphids. This yielded four groups of plants which

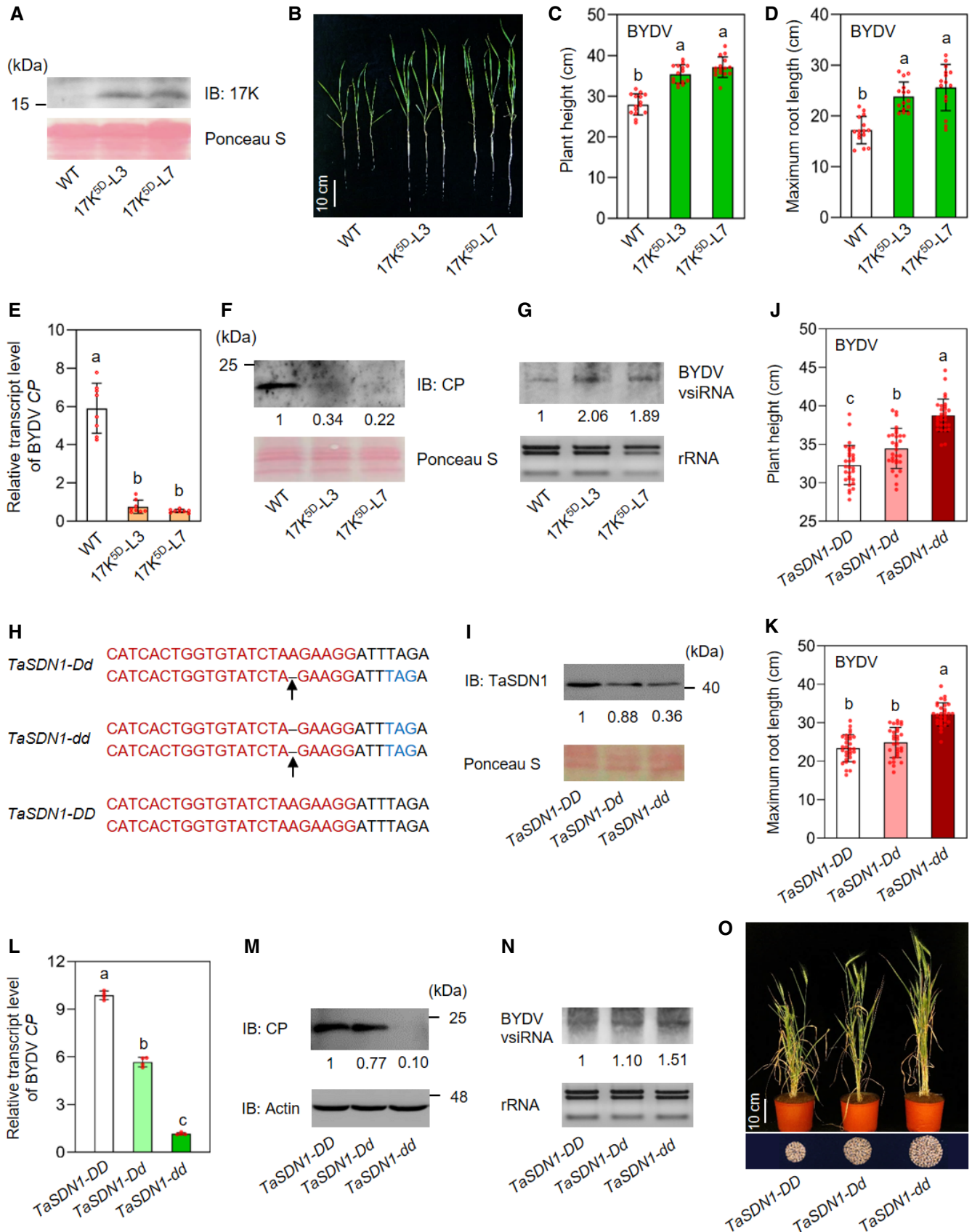


Figure 8.

**Figure 8. Genetic analysis of the function of 17K<sup>SD</sup> or SDN1 in regulating anti-BYDV RNAi in common wheat.**

- A Verification of 17K<sup>SD</sup> expression in the transgenic lines 17K<sup>SD</sup>-L3 and -L7 by immunoblotting with anti-17K antibody.
- B–D Comparison of BYDV disease symptoms including plant growth (B), plant height (C), and maximum root length (D) between two transgenic lines and WT control at 21 dpi.
- E, F The transcript (E) and protein (F) levels of viral CP gene in the BYDV-infected samples shown in (B).
- G BYDV vsRNA abundance in the set of samples shown in (B), as detected by sRNA blotting at 14 dpi.
- H CRISPR/Cas9-induced mutation in the *TaSDN1-D* homoeolog of common wheat. A single nucleotide (arrowed) was deleted in the target region (written in red), resulting in a premature stop codon (marked in blue). Selfing *TaSDN1-Dd* produced the homozygous mutant (*TaSDN1-dd*) and the plant line (*TaSDN1-DD*) homozygous for WT *TaSDN1-D*.
- I Relative to *TaSDN1-DD* line, TaSDN1 protein was decreased in *TaSDN1-Dd* and *TaSDN1-dd* mutants, with a stronger reduction found for *TaSDN1-dd*. The reactive TaSDN1 protein detected in *TaSDN1-dd* was caused by the un-mutated *TaSDN1-A* and *-B* homoeologs.
- J, K Quantitative comparison of plant height (J) and maximum root length (K) among *TaSDN1-DD*, *TaSDN1-Dd* and *TaSDN1-dd* plants at 21 dpi of BYDV.
- L, M Relative transcript (L) and protein (M) levels of BYDV CP gene in *TaSDN1-DD*, *TaSDN1-Dd* and *TaSDN1-dd* plants at 21 dpi.
- N BYDV vsRNA abundance in *TaSDN1-DD*, *TaSDN1-Dd*, and *TaSDN1-dd* plants detected by sRNA blotting at 21 dpi of BYDV.
- O The morphologies of BYDV-infected *TaSDN1-DD*, *TaSDN1-Dd* and *TaSDN1-dd* plants at adult stage, which were photographed at 20-day post anthesis. The lower panel illustrates the grain yield per plant obtained for BYDV-infected *TaSDN1-DD*, *TaSDN1-Dd* or *TaSDN1-dd*.

Data information: In (F, G, I, M, and N), the relative band intensities were obtained using ImageJ software. In (C–E and J–L), data are means  $\pm$  SD of 15 (C and D), 8 (E), 30 (J and K), or 4 (L) plants for each line, with those marked by different letters are significantly different ( $P < 0.05$ , ANOVA and LSD for multiple comparisons). The datasets shown in (A, B, F, G, I, and M–O) were all representative of three independent experiments. Source data are available online for this figure.

differed in *HvSDN1* silencing and BYDV infection: BSMV-EV/BYDV<sup>-</sup>, BSMV-SDN1gs/BYDV<sup>-</sup>, BSMV-EV/BYDV<sup>+</sup>, and BSMV-SDN1gs/BYDV<sup>+</sup>. When examined at 21 days after BYDV inoculation, BSMV-SDN1gs/BYDV<sup>+</sup> plants exhibited significantly less severe viral symptoms than those displayed by BSMV-EV/BYDV<sup>+</sup> individuals (Fig EV5B and C). As revealed by sRNA blot hybridization assays, BYDV vsRNA abundance was considerably higher in BSMV-SDN1gs/BYDV<sup>+</sup> plants than in those of BSMV-EV/BYDV<sup>+</sup> (Fig EV5D), which was confirmed by sRNA sequencing analysis (Fig EV5E and F). Judging from the transcript level of viral CP gene (Fig EV5G), BYDV proliferation was largely decreased in BSMV-SDN1gs/BYDV<sup>+</sup> plants relative to the BSMV-EV/BYDV<sup>+</sup> individuals in which *HvSDN1* was not silenced.

Second, we conducted genome editing of *TaSDN1* gene in common wheat. A single guide RNA of 20 bp was designed to edit *TaSDN1* homoeologs (*TaSDN1-A*, *-B* and *-D*, Fig EV5H) using CRISPR/Cas9 as described previously (Wang et al, 2014). After detailed screening of 273 T<sub>0</sub> wheat transformants derived from three separate genome editing experiments, only one heterozygous mutant plant (*TaSDN1-Dd*) was found, with a single, frame-shifting nucleotide deletion occurred in the mutated allele (Fig 8H). Selfing the heterozygous mutant *TaSDN1-Dd* yielded a population segregating for three genotypes, including *TaSDN1-DD* (WT segregant), *TaSDN1-Dd* (heterozygous mutant), and *TaSDN1-dd* (homozygous mutant) (Fig 8H). Compared with *TaSDN1-DD*, TaSDN1 protein level was decreased in both *TaSDN1-Dd* and *TaSDN1-dd*, with a more severe reduction found for *TaSDN1-dd* (Fig 8I). The three types of plants did not differ substantially in their growth and yield performance under normal greenhouse conditions (Appendix Fig S6). However, they showed different responses to BYDV infection based on differences in plant height and root length (Figs 8J and K, and EV5I), and in the transcript and protein levels of BYDV CP gene (Fig 8L and M), at 21 dpi. The *TaSDN1-dd* plants exhibited the highest level of BYDV resistance, because they had the largest plant height and root length values and the lowest transcript and protein levels of BYDV CP (Fig 8J–M). *TaSDN1-Dd* was also more resistant to BYDV infection than *TaSDN1-DD*, although the level of antiviral defense upregulated in *TaSDN1-Dd* was not as strong as

that in *TaSDN1-dd* (Fig 8J–M). Consistently, BYDV vsRNA abundance was higher in both *TaSDN1-Dd* and *TaSDN1-dd* than in *TaSDN1-DD*, with a much bigger increase observed for *TaSDN1-dd* (Fig 8N). The higher BYDV resistance of *TaSDN1-dd* became even more evident at 20 days post anthesis, and consequently, *TaSDN1-dd* produced substantially higher grain yield (per plant) than *TaSDN1-DD* and *TaSDN1-Dd* upon harvest (Fig 8O).

Contrary to the above findings, ectopic expression of an *HvSDN1*-GFP fusion protein in tobacco using PEBV vector led to a clear reduction in PEBV vsRNAs, which was paralleled by increased disease symptoms and elevated viral accumulation as indicated by measuring PEBV 30K and CP expression levels (Appendix Fig S7). Combined, the results depicted in Figs 8H–O and EV5 illustrate that reducing *SDN1* expression via VIGS or genome editing elevates BYDV vsRNA abundance, which leads to enhanced anti-BYDV RNAi and decreased viral proliferation in barley and wheat, respectively, whereas the opposite occurs for PEBV accumulation in tobacco cells when *SDN1* function is increased through ectopic expression of *HvSDN1*-GFP. These genetic analysis data validate the function of *SDN1* in antiviral RNAi in plant cells.

## Discussion

### BYDV 17K is phosphorylated in naturally infected host cells

In this work, we provided convincing evidence for the phosphorylation of 17K by HvGRIK1-HvSnRK1 kinases in BYDV-infected barley plants (Fig 1). Furthermore, we showed that the level of P17K was increased by overexpressing HvSnRK1-YFP but decreased by ectopically expressing a dominant-negative mutant of HvSnRK1 (i.e., HvSnRK1<sup>K139R</sup>-YFP) (Fig 2B), thus validating the phosphorylation of 17K by HvSnRK1 and the accumulation of P17K in BYDV-infected host cells. However, the band representing unphosphorylated 17K was also detected by immunoblotting (Figs 1A and 2B), indicating that both P17K and unphosphorylated 17K exist in BYDV-infected cells. Consistent with the interaction between BYDV 17K and HvSnRK1 observed in this work, Chen and colleagues recently

reported the interaction between BYDV 17K and tobacco SnRK1 in yeast cells (Chen *et al*, 2021a), but they did not present any evidence on the functional significance of this interaction. Notably, the 17K protein encoded by the polerovirus, potato leaf roll virus (PLRV), has been shown to be phosphorylated on multiple serine residues (S71, S79, S137, and S140) (Tacke *et al*, 1993; Link *et al*, 2011), although the host kinase(s) involved remain to be identified. Comparison of amino acid sequences indicated that the S137 residue of PLRV 17K matches S132 of BYDV-GAV 17K (Appendix Fig S8). Considering the finding of S132 phosphorylation by HvSnRK1 in this work (Fig 1E and F), it is worthy to test whether the GRIK1-SnRK1 kinases may also be involved in PLRV 17K phosphorylation.

Similar to our work, previous studies have reported SnRK1-mediated phosphorylation of the VSRs encoded by several DNA genome containing geminiviruses, which include the  $\beta$ C1 protein of tomato yellow leaf curl China virus (TYLCCNV) (Shen *et al*, 2011; Zhong *et al*, 2017; Shen & Hanley-Bowdoin, 2020) and the AL2/C2 protein of cabbage leaf curl virus (CaLCuV) and tomato mottle virus (ToMoV) (Shen *et al*, 2014, 2018; Shen & Hanley-Bowdoin, 2020). Based on our work and the previous studies, it is clear that GRIK1-SnRK1 kinases can phosphorylate the VSRs expressed by either RNA or DNA viruses that infect monocot or dicot plants. However, we find for the first time that HvGRIK1 alone can phosphorylate 17K VSR *in vitro*, indicating that GRIK1 may play a dual role in the phosphomodification of plant viral proteins by GRIK1-SnRK1 kinase cascade, that is, activation of SnRK1 kinase activity and direct phosphorylation of substrate VSR proteins by itself. This information will help to stimulate deeper analysis of the function of GRIK1-SnRK1 kinases in plant virus–host interactions in future research.

Nevertheless, the interplay between the HvGRIK1-HvSnRK1 kinase cascade and BYDV 17K protein in host plants may be more complex than revealed so far. Here, we focused on analyzing the phosphorylation of 17K by HvSnRK1 and its effect on anti-BYDV RNAi because of the availability of transgenic barley lines with altered levels of HvSnRK1 kinase activity (Han *et al*, 2020b). Further research is needed to understand the involvement of HvGRIK1 in the regulation of 17K function in BYDV-infected plants as it interacts with 17K and can phosphorylate two residues of 17K alone *in vitro* (Fig 1C and E). Moreover, it will also be interesting to explore the effects of 17K binding on the biochemical and physiological functions of HvGRIK1-HvSnRK1 kinases in regulating plant growth and development, because it has been shown that some plant viral proteins can inactivate host SnRK1 and adenosine kinases through protein–protein interactions (Hao *et al*, 2003; Wang *et al*, 2003). Finally, although our TriFC assays indicated that (PM)-17K-RN, RC-HvGRIK1-VC, and HvSnRK1-VN may form a protein complex in tobacco cells, additional experiments are required to verify whether 17K, HvGRIK1, and HvSnRK1 indeed form a three-protein complex in BYDV-infected host cells.

It is well known that the SNF1-related kinase family of higher plants has multiple members with diverse functions (Halford & Hey, 2009; Chen *et al*, 2021b). So another question worthy of future investigation is to examine whether other types of SnRK proteins may also interact with BYDV 17K and take part in its phosphorylation. In a preliminary experiment, we found that HvPKABA1, a SnRK2 protein (Holappa & Walker-Simmons, 1995; Chen *et al*, 2021a, 2021b), interacted with 17K in both Y2H and LC

assays; but HvCIPK1, a SnRK3 protein (Hrabak *et al*, 2003; Chen *et al*, 2021a, 2021b), failed to do so in the same tests (Appendix Fig S9A and B). Notably, compared with HvCIPK1, HvPKABA1 exhibited lower amino acid sequence identities with HvSnRK1 in both full-length protein and kinase domain (Appendix Fig S9C and D); hence, we speculate that BYDV 17K may interact with additional SnRK proteins in a highly selective manner in host cells, and that HvPKABA1 may also participate in 17K phosphorylation during BYDV infection. This may not be surprising as it has been demonstrated that certain plant viral protein, such as the  $\gamma$ B VSR protein of BSMV, can be phosphorylated by multiple kinases in host plants, that is, a PKA-like kinase (Zhang *et al*, 2018) and a serine/threonine/tyrosine kinase STY46 (Zhang *et al*, 2021). Remarkably, phosphorylation by PKA-like kinase was required for  $\gamma$ B's VSR activity (Zhang *et al*, 2018), while that by STY46 kinase did not affect  $\gamma$ B's VSR activity but undermined BSMV's replication in host cells (Zhang *et al*, 2021). These insights highlight the fact that a plant viral protein can be phosphorylated by different kinases in host plants with complex consequences on its function in viral pathogenesis.

#### Phosphorylated 17K upregulates antiviral RNAi via enhancing vsiRNA abundance

We showed that overexpressing HvSnRK1-YFP increased the level of P17K, elevated vsiRNA abundance, lowered virus proliferation, and attenuated viral symptoms in BYDV-infected barley, whereas the reverse was observed for the plants ectopically expression HvSnRK1<sup>K139R</sup>-YFP (Figs 2 and 3). These data suggest that P17K upregulates antiviral gene silencing via enhancing vsiRNA accumulation in BYDV-infected cells. Consistent with this result, 17K<sup>5D</sup> (a phosphomimic mutant of 17K), but not 17K<sup>5A</sup> (a dephosphomimic mutant of 17K), enhanced tobacco resistance to PEBV infection accompanied by enhanced accumulation of PEBV-derived vsiRNAs (Fig 4). In contrast to 17K and 17K<sup>5A</sup>, 17K<sup>5D</sup> did not show detectable VSR activity (Fig 4). Thus, phosphorylation of 17K by HvGRIK1-HvSnRK1 kinases disrupts its VSR function, with the phosphorylated 17K (P17K) acquiring the ability to promote anti-BYDV RNAi via elevating vsiRNA abundance.

The SnRK1-phosphorylated  $\beta$ C1 protein of TYLCCNV also loses VSR activity (Zhong *et al*, 2017), but it remains to know whether the phosphomodification of  $\beta$ C1 or the AL2/C2 proteins of CaLCuV and ToMoV by SnRK1 may enable them to promote antiviral gene silencing. From the insight generated here for BYDV P17K, it will be interesting to examine whether the geminivirus VSRs phosphorylated by SnRK1 may also gain the ability to upregulate antiviral RNAi via enhancing vsiRNA accumulation.

#### Phosphorylated 17K inhibits HvSDN1-mediated vsiRNA cleavage, thereby enhancing vsiRNA accumulation

What is the mechanism underlying the enhancement of vsiRNA accumulation by P17K in BYDV-infected host cells? From the molecular, biochemical, and genetic data presented in Figs 5–8, we propose that P17K enhances vsiRNA accumulation via inhibiting the cleavage of HvAGO1-carried vsiRNAs by HvSDN1. This suggestion is supported by five lines of evidence. First, 17K<sup>5D</sup> (a phosphomimic mutant of 17K), but not the unphosphorylated 17K, interacted with

HvSDN1 and inhibited vsiRNA cleavage by recombinant HvSDN1 *in vitro* (Figs 5A and B, and 6B). Second, in BYDV-infected barley plants, P17K and BYDV vsiRNA accumulated to a higher amount in cells with increased SnRK1 function compared to those with decreased SnRK1 activity or WT cells (Figs 2B and 3A and B). Third, as revealed by analyzing the immunoprecipitates prepared with anti-HvAGO1 antibody, P17K, HvAGO1, HvSDN1, and BYDV vsiRNA coexisted in the same complex, with the amount of vsiRNAs associated with HvAGO1 being positively correlated with the accumulation level of P17K (Fig 7B). Fourth, HvAGO1 and HvSDN1 interacted with each other in Y2H assays (Fig 7A) and in BYDV-infected cells (Fig 7B and C). Therefore, we deduce that HvSDN1 degrades BYDV vsiRNAs carried by HvAGO1 via interacting with HvAGO1, but this degradation is inhibited by P17K, which is especially evident in the SnRK1-YFP-L4 plants with increased level of P17K accumulation (Fig 7B). Finally, we validated the function of P17K in promoting anti-BYDV RNAi and the role of HvSDN1 in cleaving vsiRNAs *in planta* by conducting genetic experiments (Figs 8 and EV5).

The molecular processes contributing to the impediment of HvSDN1-catalyzed vsiRNA cleavage by P17K in BYDV-infected host cells are likely complex. From the evidence gathered in this work, we suggest that at least two processes may be involved. First, direct inhibition of HvSDN1 enzyme activity by P17K. This is possible because 17K<sup>5D</sup> interacted with HvSDN1 and inhibited vsiRNA cleavage by recombinant HvSDN1 *in vitro* (Fig 6) and P17K coexisted with HvSDN1 in the same complex *in vivo* (Fig 7B). Second, P17K weakens the interaction between HvSDN1 and vsiRNA-carrying HvAGO1 (Fig 7B–D), which may decrease the efficiency of HvSDN1 to get access to, and then to degrade, the vsiRNAs carried by HvAGO1. Hence, in BYDV-infected cells, 17K is phosphorylated by upregulated HvGRIK1-HvSnRK1 kinase function, with the resulting P17K acquiring the ability to bind HvSDN1, HvAGO1, and vsiRNA. This may enable P17K to directly inhibit HvSDN1 enzyme activity and to weaken the interaction between HvSDN1 and HvAGO1, which together downregulate the degradation of HvAGO1-associated vsiRNAs by HvSDN1, thus enhancing vsiRNA abundance and anti-BYDV RNAi (Fig 9). Binding of P17K to vsiRNAs might protect them from cleavage by HvSDN1, thus also contributing to vsiRNA abundance and antiviral RNAi, but further evidence is needed to support this possibility.

In contrast to P17K, the unphosphorylated 17K (17K), an important virulence protein in BYDVs (Nass *et al*, 1998; Fusaro *et al*, 2017; Jin *et al*, 2020), suppresses antiviral gene silencing likely by debilitating the function of HvAGO1 (as evidenced by its binding to HvAGO1, Fig 7A and B). But the VSR function of 17K is counteracted by P17K that enhances anti-BYDV RNAi through elevating vsiRNA abundance. Conversion of 17K to P17K by HvGRIK1-HvSnRK1 kinases may also negatively affect the function of 17K in BYDV pathogenesis because of reduction in the amount of 17K (Fig 9). Nevertheless, we speculate that in the early stage of BYDV infection, the VSR activity of 17K is dominant, thus allowing the establishment of viral infection. As infection proceeds, the amount of P17K increases due to upregulation of HvGRIK1-HvSnRK1 kinase function, which results in an enhancement of anti-BYDV RNAi. Finally, the simultaneous functions of 17K and P17K could lead to successful BYDV infection but with controlled viral proliferation, thus benefiting the long-term co-survival of BYDV and its host in

nature (Fig 9). The occurrence and function of P17K define a novel mechanism that enhances antiviral RNAi through host subversion of a viral virulence protein to inhibit vsiRNA degradation by SDN1 enzyme. To our knowledge, host subversion of virus protein to regulate viral proliferation has not been reported in past studies, although viral subversion of host proteins for their amplification in infected cells is a common phenomenon (Walsh & Mohr, 2011; Hernandez-Gonzalez *et al*, 2021).

Further to revealing the complex containing P17K, HvSDN1, and HvAGO1 in BYDV-infected host cells by Co-IP assays (Fig 7), it is relevant to ask in which cellular compartment this complex forms and functions. By analyzing the cytosolic and nuclear protein samples prepared from BYDV-infected tissues with immunoblotting (Feys *et al*, 2005), we found that 17K, P17K, activated HvSnRK1 (i.e., phosphorylated SnRK1, Fig 1B), HvSDN1, and HvAGO1 were all present in cytosolic proteins (Appendix Fig S10), thus making it possible for the activated HvSnRK1 to phosphorylate 17K, 17K to interact with HvAGO1, and P17K to interact with HvAGO1 and HvSDN1 in the cytoplasm. Consistent with previous studies (Fang & Qi, 2016; Martínez-Barajas & Coello, 2020), activated SnRK1, as well as AGO1, were also found in the nucleus in this work (Appendix Fig S10), whose functions in regulating BYDV pathogenesis merit further studies. But judging from the predominant presence of 17K, P17K, and HvSDN1 in the cytoplasm (Appendix Fig S10), we propose that phosphorylation of 17K by activated HvSnRK1, interaction of 17K with HvAGO1, and interaction among P17K, HvAGO1 and HvSDN1 occur mainly in the cytoplasm in BYDV-infected barley.

It is worth noting that 17K<sup>5D</sup>, but not 17K, were found to bind BYDV vsiRNA (Fig 5C) in this work. Although vsiRNA binding has been shown important for the function of many plant viral VSRs (Vargason *et al*, 2003; Lakatos *et al*, 2006; Li & Wang, 2019; Annacchia & Martinez, 2021), there are also VSRs that do not bind vsiRNA (Csorba *et al*, 2010; Fernández-Calvino *et al*, 2016). For example, the P0 VSRs of cucurbit aphid-borne yellows virus and beet western yellows virus do not bind vsiRNA; they suppress host antiviral RNAi through mediating the degradation of AGO proteins (Bortolamiol *et al*, 2007; Csorba *et al*, 2010). Hence, BYDV 17K joins the VSRs that counteract host antiviral RNAi without needing to bind vsiRNA. On the contrary, 17K<sup>5D</sup> could bind BYDV vsiRNA, and this activity was required for its efficient inhibition of vsiRNA cleavage by recombinant HvSDN1 (Fig 6C–H). Therefore, vsiRNA binding may be involved in the impediment of HvSDN1-catalyzed vsiRNA cleavage by P17K in BYDV-infected cells.

### New ways for engineering BYDV-resistant crops

Despite being studied for more than six decades, BYDVs still cause serious economic losses in cereal crops worldwide (Ali *et al*, 2018; Heck & Brault, 2018; Aradottir & Crespo-Herrera, 2021). The development of BYDV-resistant varieties by conventional breeding is time-consuming and labor intensive, and innovative approaches are desirable for efficiently developing BYDV-resistant lines (Heck & Brault, 2018; Aradottir & Crespo-Herrera, 2021). Concomitant to revealing the promotion of anti-BYDV RNAi by P17K and the underlying mechanism, we found that the transgenic lines ectopically expressing 17K<sup>5D</sup> and the *SDN1* mutant produced by genome editing exhibited significantly improved tolerance to BYDV infection (Fig 8), thus providing new ways for engineering BYDV-resistant

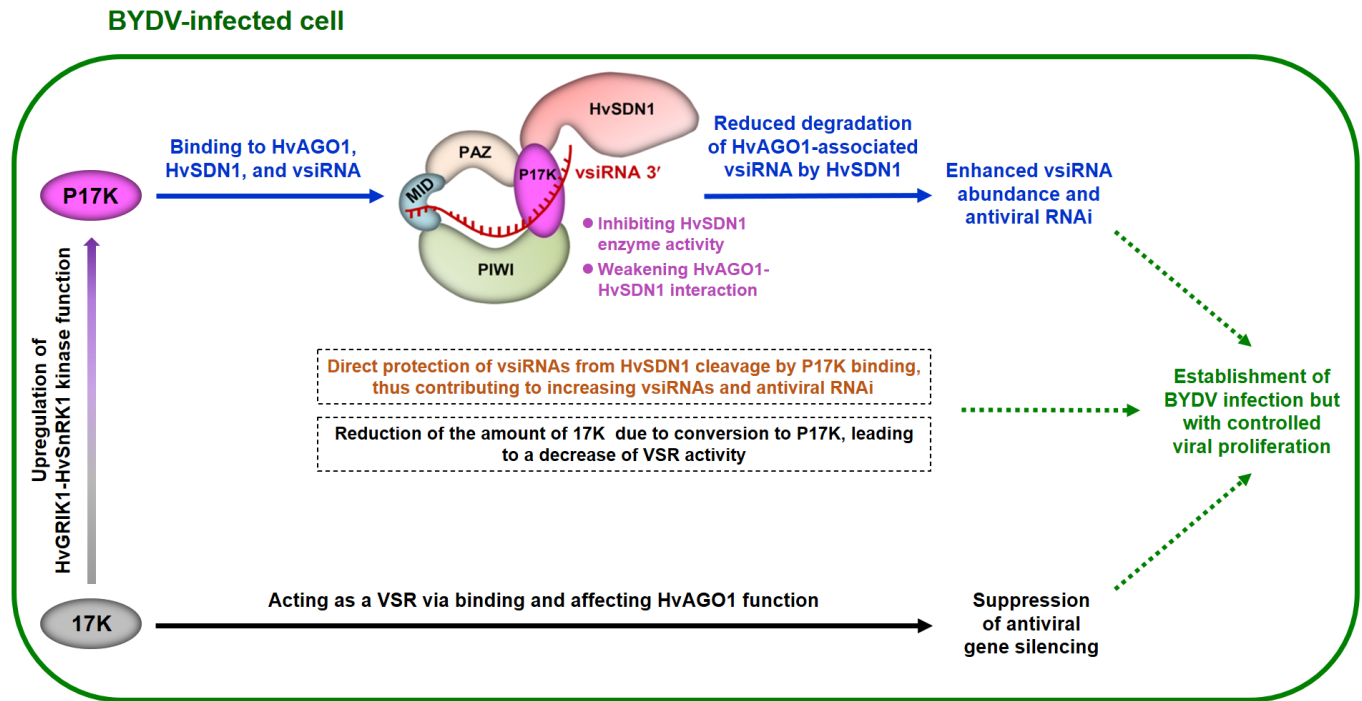


**Figure 9. A working model on the enhancement of vsiRNA abundance and antiviral RNAi by phosphorylated 17K (P17K) in BYDV-infected host cell.**

Upregulation of HvGRK1-HvSnRK1 kinase function results in the accumulation of phosphorylated 17K (P17K), which binds HvSDN1, HvAGO1, and vsiRNA. This may enable P17K to directly inhibit HvSDN1 enzyme activity, thus impeding HvSDN1-catalyzed vsiRNA cleavage. Moreover, P17K weakens the interaction between HvSDN1 and HvAGO1, hampering the cleavage of vsiRNAs carried by HvAGO1. Both processes may contribute to reduced degradation of HvAGO1-associated vsiRNAs by HvSDN1, thus enhancing vsiRNA abundance and antiviral RNAi. Binding of P17K to vsiRNAs might protect them from cleavage by HvSDN1, thus also contributing to vsiRNA abundance and antiviral RNAi, but further evidence is needed to support this possibility. On the other hand, the unphosphorylated 17K (17K), being a VSR, suppresses antiviral gene silencing probably by debilitating the function of HvAGO1. The change of 17K to P17K lowers the amount of 17K in the BYDV-infected barley cells, which probably decreases the total VSR activity of 17K and potentially increases the strength of host antiviral gene silencing. Simultaneous functions of 17K and P17K could finally lead to the establishment of BYDV infection while avoiding excessive viral proliferation, which might benefit the long-term co-survival of BYDV and its host in nature. The occurrence and function of P17K define a previously unreported antiviral mechanism augmented by host subversion of a viral virulence protein to inhibit vsiRNA degradation by SDN1 enzyme. The HvAGO1-HvSDN1-P17K complex is drawn based on the data gathered in this work, with consideration of the structural information published for *Arabidopsis* SDN1 (Chen *et al.*, 2018).

crops. The *TaSDN1-dd* mutant line, showing heightened BYDV resistance (Fig 8H–O), may represent a valuable genetic resource for innovative control of BYDV epidemics in global wheat production. Additionally, the *TaSDN1-dd* mutant also exhibited improved resistance to another wheat-infecting virus, BSMV (Appendix Fig S11), indicating that decreasing *TaSDN1* expression may be useful for producing the wheat lines with broad-spectrum virus resistance. As *SDN1* homologs exist in both plants and animals (Ramachandran & Chen, 2008; Yu *et al.*, 2017; Chen *et al.*, 2018), manipulating *SDN1* expression by genome editing may be broadly applicable for engineering virus resistance in important crops and animals.

Apart from conferring BYDV resistance in transgenic common wheat (Fig 8H–O), ectopic expression of 17K<sup>5D</sup> also increased the resistance of *N. benthamiana* to PEBV accompanied by enhanced accumulation of PEBV-derived vsiRNA (Fig 4C–F). Further tests showed that 17K<sup>5D</sup> expression could also elevate tobacco resistance to potato virus X or BSMV (Appendix Fig S12). As a phosphomimic mutant of 17K, 17K<sup>5D</sup> may use a similar mechanism as P17K to enhance vsiRNA accumulation and antiviral RNAi through binding to the AGO1 and SDN1 proteins that are conserved in higher plants. Therefore, it is worthwhile to explore the utility of 17K<sup>5D</sup> in

developing broad-spectrum antiviral resistance in crops. Considering that 17K is conserved in polioviruses (Ali *et al.*, 2018; Heck & Brault, 2018), the insights obtained in this work may aid the functional study of polioviral 17K protein, thus resulting in new strategies for controlling the diseases elicited by diverse polioviral pathogens.

In summary, we have discovered a novel mechanism that promotes antiviral RNAi. It is triggered by functional subversion of a viral virulence protein (i.e., BYDV 17K) through host-mediated phosphomodification, and this mechanism contributes significantly to the control of viral proliferation in infected cells. Our work generates new knowledge on antiviral RNAi, which can be exploited to engineer virus resistance in crop plants (e.g., BYDV resistance in wheat and barley).

## Materials and Methods

### Plant materials and inoculation of BYDV

Wild-type barley (cv. Golden Promise), transgenic barley expressing 17K-GFP, and SnRK1-YFP and SnRK1<sup>K139R</sup>-YFP transgenic lines were

described previously (Jin *et al.*, 2020; Han *et al.*, 2020b). They were germinated at 23°C for 5 days, with uniformly developed seedlings selected and cultured in a hydroponic device containing Hoagland nutrient solution. The whole device was transferred into the growth chamber with a day/night temperature regime of 24°C/20°C and a photoperiod of 16-h light/8-h dark. One day after transfer, the seedlings were inoculated with the aphids (*Schizaphis graminum*) carrying, or free of, BYDV-GAV (Jin *et al.*, 2020). The aphids were killed by adding imidacloprid to the nutrient solution (at 2 mg/L) at 4 days after inoculation. The barley plants were then phenotyped or sampled at appropriate time points. *N. benthamiana*, including WT strain and 16c transgenic line (Yaegashi *et al.*, 2012), was grown in the greenhouse at 23°C with a photoperiod of 16-h light/8-h dark, and used as desired.

### Gene constructs and antibodies

The oligonucleotide primers and probes used in this study were listed in Appendix Table S2. The gene constructs and various antibodies used in this work were described in Appendix Tables S3 and S4, respectively.

### Phos-tag SDS-PAGE coupled immunoblotting assays

These assays were employed to detect phosphorylated 17K (P17K) as described previously (Kinoshita *et al.*, 2016) with some modifications. Specifically, after Phos-tag SDS-PAGE, we used the electrotransfer buffer containing 10 mM EDTA to rinse the gel three times (rather than using the electrotransfer buffer containing 1 mM EDTA to rinse the gel once in the original method) before electrotransfer of separated proteins to PVDF membrane, which not only increased the efficiency of protein transfer but also decreased the background of immunoblotting. For detecting P17K in BYDV-infected barley, the samples were collected at desired time points and ground in liquid nitrogen, with total proteins extracted using the lysis buffer containing 1× protease inhibitor cocktail (Roche, Cat# 11836170001) and 1× PhosSTOP inhibitor cocktail (Roche, Cat# 4906837001). These protein samples were clarified by centrifugation for 10 min (18,200 g) at 4°C. The supernatants were either directly analyzed in Phos-tag SDS-PAGE or analyzed after treatment with λ-protein phosphatase (λ-PP, New England Biolabs, Cat# P0753) for 30 min at 30°C as detailed in our previous study (Jin *et al.*, 2020). For detecting P17K in the *in vitro* kinase assays, the reaction mixtures were directly analyzed in Phos-tag SDS-PAGE. After protein separation, 17K and P17K were revealed using immunoblotting with a polyclonal antibody specific for BYDV 17K (Appendix Table S4). For visualizing P17K associated with HvAGO1, the immunoprecipitates, prepared using HvAGO1 antibody (see below), were directly separated in Phos-tag SDS-PAGE following by immunoblotting with anti-17K antibody.

### RNA extraction and qRT-PCR assays

Total RNA samples were prepared from the collected plant materials using the TriPure Isolation Reagent (Roche, Cat# 94012520). They were converted to cDNAs with the GoScript™ Reverse Transcription System (Promega, Cat# A5000). The resultant cDNAs were then used in quantitative PCR assays with gene-specific primers

(Appendix Table S2). The *Actin* gene was amplified as an internal control.

### Y2H assays

Yeast two-hybrid (Y2H) assays were performed using the pB42AD and pLexA vectors according to the manufacturer's instructions (Clontech, www.clontech.com). The bait and prey constructs were co-transformed into the yeast strain EGY48 (MATa, *his3*, *trp1*, *ura3*, LexAop(x6)-LEU1 Plus p8op-lacZ). The positive colonies were screened by growing them on the SD-Ura/-His/-Trp media for 3 days at 30°C, which were further verified on the SD/Gal/Raf/-Ura/-His/-Trp/-Leu media containing X-β-Gal. The primers used in Y2H assays were listed in Appendix Table S2.

### LC assays

Luciferase complementation (LC) assays were accomplished essentially as described previously (Chen *et al.*, 2008). The pCAMBIA1300-nLUC and pCAMBIA1300-cLUC vectors were employed to express the N- or C-terminal luciferase-fusion proteins (Appendix Table S3) to be examined for protein-protein interactions. The primers used for the cloning were listed in Appendix Table S2. The LUC signals were detected in a luminescence imaging system (Berthold) with an exposure time of 2–10 min.

### Co-IP assays

These assays were performed to detect protein-protein interactions in various barley samples essentially as described in our previous study (Jin *et al.*, 2020). Briefly, total proteins, extracted from desired barley tissues, were centrifuged for 15 min (18,200 g) at 4°C. The resultant supernatants were filtered through Miracloth (Merck Millipore), followed by an overnight incubation (at 4°C) with the GFP-Trap magnetic beads (Chromotek, Cat# gtma-20) (for detecting the interaction between 17K-GFP and HvSnRK1) or the protein A/G magnetic beads cross-linked with HvAGO1 or HvSDN1 antibodies. Subsequently, the beads were collected and washed four times with a washing buffer. The protein complexes were eluted by boiling the beads in 2× SDS-PAGE sample buffer for 5 min, which were then separated using 12% SDS-PAGE, followed by immunoblotting with appropriate antibodies (Appendix Table S4).

### TriFC assays

Dual-color trimolecular fluorescence complementation (TriFC) analysis was performed according to a previous study (Offenborn *et al.*, 2015). Briefly, the coding sequences of 17K, PM-17K, HvGRIK1, and HvSnRK1 were amplified by RT-PCR with desired oligonucleotide primers (Appendix Table S2) and cloned into pSmRYNE, pStriRV, and pVYNE vectors to express 17K-RN, (PM)-17K-RN, RC-HvGRIK1-VC, and HvSnRK1-VN fusions, respectively (Appendix Table S3). The four constructs were each introduced into the *Agrobacterium* strain GV3101. The resultant *Agrobacterium* cultures were then infiltrated into *N. benthamiana* leaves in desired combinations. The fluorescent signals generated were examined at 60-h post agroinfiltration under a confocal microscope (Carl Zeiss LSM980). To examine plasma membrane association of the yellow

fluorescence due to the formation of a protein complex by (PM)-17K-RN, RC-HvGRIK1-VC, and HvSnRK1-VN, the cells co-expressing the three proteins were plasmolyzed with 1 M mannitol for 30 min at 25°C before confocal microscopy. The excitation and emission wavelengths employed to detect the fluorescent proteins were 514 nm/527 nm for Venus and 543 nm/610 nm for mCherry. For examining the colocalizations of green and red signals, the images were taken using the best signal model with bidirectional scanning. All images were collected with a confocal pinhole of 1 arbitrary unit using a 20× objective.

### Protein expression and purification

Briefly, the pGEX4T-1, pET30a, or pET32a vectors were used to express the GST fusions or His-tagged proteins (Appendix Table S3) used in this study. The preparation of bacterial expression constructs, induction of protein expression, and purification of recombinant proteins were executed as detailed in the report (Han et al, 2020b). The primers used in the cloning were described in Appendix Table S2.

### In vitro kinase assay and LC-MS/MS analysis

In vitro kinase assays were performed as previously described (Shen et al, 2011). Five recombinant proteins, GST-HvGRIK1, GST-HvSnRK1-KD, GST-17K, GST-17K<sup>3A</sup>, and GST-17K<sup>5A</sup>, were used in appropriate combinations. The reaction mixtures (50 µl each) were incubated at 30°C for 30 min and were stopped by adding 4× SDS-PAGE sample buffer. After boiling for 5 min, the mixtures (20 µl each) were separated using 12% Phos-tag SDS-PAGE, followed by immunoblotting with anti-17K antibody as detailed previously (Jin et al, 2020). For LC-MS/MS analysis, the mixtures of phosphorylation reactions were separated in 12% SDS-PAGE followed by Coomassie blue staining. The GST-17K bands in different phosphorylation reactions were excised from the stained gel and were subjected to LC-MS/MS analysis as outlined in the work (Han et al, 2020b).

### Small RNA sequencing

Small RNA (sRNA) sequencing was performed commercially (Novogene Co. Ltd., Beijing, China). Three biological replicates were sequenced for each sample. The sequencing libraries were generated using the kit NEBNext® Multiplex Small RNA Library Prep Set for Illumina® (New England Biolabs) based on the manufacturer's recommendations. Briefly, the sRNAs were converted to cDNAs through reverse transcription using the oligonucleotide primers with built-in adaptors, which facilitated subsequent amplification by PCR. The resulting products were separated in polyacrylamide gel, with the sRNA bands excised. After gel extraction, the sRNAs were used to prepare sequencing libraries, which were sequenced on the Illumina HiSeq2500 platform to generate 50 bp short reads. The raw data reads were initially trimmed with the cutadapt program (version 1.18) to remove Illumina adapters and low-quality bases (quality score < 30). The resultant reads with the length of 18–30 nt were retained and normalized by the total reads. To analyze the expression of vsiRNA, the bowtie program (version 1.2.3) was applied for mapping the 21–24 nt sequencing reads to the genome

of BYDV or PEBV, the unique mapped reads were considered as valid vsiRNAs and used in further analysis.

### VSR activity assays

The VSR activity assays were conducted according to previously described protocol (Yaegashi et al, 2012). The coding sequences of 17K, 17K<sup>5A</sup>, and 17K<sup>5D</sup> were each cloned into the pEG100 vector (Appendix Table S3) using Gateway technology (Invitrogen). The constructs were individually transformed into the *Agrobacterium* strain GV3101 (Biomed). Then, the *Agrobacterium* strain carrying 35S::GFP and those designed to express 17K, 17K<sup>5A</sup>, or 17K<sup>5D</sup> were co-infiltrated into the leaves of the 16c transgenic tobacco plants. Two additional *Agrobacterium* strains carrying the empty vector pEG100 or the 35S::P19 construct designed to express the P19 VSR of TBSV were used as negative and positive controls, respectively. Green fluorescence signals were visualized at 4-day post *Agrobacterium* infiltration using a handheld long-wavelength UV lamp (Blak-Ray B-100AP, Ultraviolet Products). The RNA and protein levels of GFP were examined using qRT-PCR or immunoblotting assays. The siRNAs of GFP were detected using sRNA blotting assays (see below).

### Small RNA blotting assays

Preparation of total RNA samples and their separation in polyacrylamide gels were accomplished as documented previously (Huang et al, 2019). After transfer to Hybond N<sup>+</sup> membranes, the blots were hybridized with non-radioactive probes specific for the siRNAs of GFP or the vsiRNAs of PEBV or BYDV. The probes were prepared by *in vitro* transcription in the presence of digoxigenin-labeled UTP following the manufacturer's instruction (DIG Northern Starter Kit, Sigma-Aldrich). The templates used in *in vitro* transcription reactions were the plasmid clones (Appendix Table S3) carrying the coding sequence of GFP or the genomic RNA sequence of PEBV or BYDV linearized with the restriction enzyme *SpeI*. The hybridization was performed following the protocol of DIG Northern Starter Kit (Roche, Cat# 12039672910). After the hybridization, the blots were washed two times with high stringency buffer (2× SSC containing 0.2% SDS). After blocking, the blots were incubated with the anti-digoxigenin antibody-AP conjugate for 30 min at 25°C, with the hybridization signals developed using the substrate CDP-Star.

For detecting BYDV vsiRNAs associated with HvAGO1, vsiRNAs were extracted from the immunoprecipitates prepared using anti-HvAGO1 antibody and separated in polyacrylamide gel (Huang et al, 2019), followed by blotting, hybridization, and signal detection as outlined above.

### Ectopic expression of 17K, 17K<sup>5A</sup>, 17K<sup>5D</sup>, or HvSDN1-GFP in tobacco using the PEBV vector

Pea early browning virus (PEBV)-based vector (Constantin et al, 2004) was employed to express 17K, 17K<sup>5A</sup>, 17K<sup>5D</sup>, or HvSDN1-GFP in *N. benthamiana* plants following the method reported previously (Jin et al, 2020). As a control, free GFP was also expressed using PEBV vector. The coding sequences of 17K, 17K<sup>5A</sup>, 17K<sup>5D</sup>, or HvSDN1-GFP were each cloned into PEBV vector by infusion cloning technology with appropriate primers listed in Appendix Table S2. The recombinant PEBVs were each introduced into the leaves of 35

*N. benthamiana* plants via agroinfiltration. The same number of plants was infiltrated with sterile water as controls. The accumulation levels of PEBVs in tobacco leaves were monitored by qRT-PCR and immunoblotting assays of viral CP transcripts and protein, respectively. The antibody specific for PEBV CP was described before (Wang & Maule, 1997).

### Activity assays of recombinant HvSDN1

For the activity assays using biotin-labeled substrate, vsiRNA899 was labeled by biotin at the 5' end by reacting with the hydroxide group (Beijing SYKM Gene Biotechnology Co. Ltd., Beijing, China). In the activity assays using fluorogenic substrate, vsiRNA899 was labeled by FAM (carboxyfluorescein) at the 5' end by reacting with the hydroxide group and by TAMRA (carboxytetramethylrhodamine) at the 3' end through reacting with NH<sub>2</sub> (Beijing SYKM Gene Biotechnology Co. Ltd.). The assay reactions (20 µl each) were set up as reported previously (Ramachandran & Chen, 2008).

Briefly, in each reaction, 1 µg of His-HvSDN1 was incubated with 100 nM vsiRNA substrate (in the presence of GST-17K or GST-17K<sup>5D</sup>) at 37°C for 30 min in an incubator or a PCR machine (see below). Afterward, three methods were used to detect the cleavage products. First, the cleavage products of biotin-labeled vsiRNA were separated in 17% denaturing polyacrylamide gel, followed by transfer to Hybond N<sup>+</sup> membrane, with the signals detected using the protocol detailed in the LightShift™ Chemiluminescent RNA EMSA Kit (Thermo Fisher Scientific, Cat# 20158). This method permitted direct visualization, but not accurate quantification, of cleavage products. Second, a Typhoon FLA9500 laser scanner (GE healthcare) was used to quantify FAM fluorescence in each reaction, which reflected the amount of vsiRNA cleaved. An aliquot (3 µl) of the reaction mixture, spotted on a laminating film, was scanned by Typhoon FLA9500. This method was simple, and permitted relative comparison of FAM fluorescence levels (indicating the amounts of substrate cleaved) generated in different reactions. Third, the activity assay was conducted in 96-well plates in a real-time quantitative PCR platform (Roche LC 480) for 30 min at 37°C, with the level of FAM fluorescence recorded for each reaction. To quantify the amount of vsiRNA cleaved, a standard curve was established using a set of reactions each containing 4 µg of His-HvSDN1 but with variable amounts of fluorogenic vsiRNA substrate (Fig EV3B). This method was simple, rapid, and high-throughput, and allowed more accurate quantification of the vsiRNA substrate cleaved in different reactions. As controls for the activity assays using biotin-labeled vsiRNA, His-HvSDN1 was replaced by GST protein, or missed in the reaction (Fig 6A). In the activity assays using fluorogenic vsiRNA substrate, each assay had a corresponding control that lacked His-HvSDN1 in the reaction mixture, whose FAM fluorescence value was used to remove background signal.

### Small RNA binding assays

Small RNA binding assays were performed using LightShift™ Chemiluminescent RNA EMSA Kit (Thermo Fisher Scientific, Cat# 20158). A 21 nt vsiRNA (vsiRNA899, Appendix Table S2) derived from BYDV genome was synthesized and labeled by biotin at the 3' end (Beijing SYKM Gene Biotechnology Co. Ltd.) as the probe. The proteins used in the RNA binding assays included GST (as control),

GST-17K, GST-17K<sup>5D</sup>, GST-17K<sup>5D</sup>m4, GST-17K<sup>5D</sup>m2a, and GST-17K<sup>5D</sup>m2b, which were purified as described above. The probe and the protein were mixed in the binding buffer for 30 min at room temperature. Afterward, the reaction products were separated using 9% native PAGE in 0.5× TBE buffer followed by transfer to Hybond N<sup>+</sup> membranes for 40 min at 400 mA. The blots were cross-linked under UV light for 3 min, with the remaining steps conducted according to the protocol detailed in the RNA EMSA Kit. Unlabeled vsiRNA899 was used as a competitor and added to the reaction containing GST-17K<sup>5D</sup> to test the strength of the binding. The binding assay was also carried out using a vsiRNA duplex probe, which was prepared by mixing the biotin-labeled vsiRNA899 with its unlabeled antisense counterpart (with 2 bp overhang at the 3' end) in a 1:1 molar ratio. The duplex was formed by annealing at 95°C for 10 min followed by gradual cooling to 25°C.

### Development and analysis of 17K<sup>5D</sup> transgenic lines

The T-DNA construct pLH5-Ubi::17K<sup>5D</sup>, prepared using the infusion technology with the primers containing *SacI* restriction endonuclease sites (Appendix Table S2), was employed to develop the transgenic lines expressing 17K<sup>5D</sup> by *Agrobacterium*-mediated transformation of the spring wheat cultivar Fielder (Wang et al, 2017). Two independent lines (17K<sup>5D</sup>-L3 and -L7) were analyzed for BYDV resistance and vsiRNA abundance with WT Fielder as control. Plant culture, BYDV inoculation, assessment of viral symptoms and virus proliferation, and measurement of vsiRNA abundance by sRNA blotting were conducted as detailed above.

### BSMV induced gene silencing

Barley stripe mosaic virus-mediated silencing of *HvSDN1* was carried out as previously described (Yuan et al, 2011). In brief, the 117 bp fragment of *HvSDN1* coding sequence was amplified by RT-PCR using the desired primers (Appendix Table S2), followed by cloning into pCa-γbLIC vector to obtain pCa-γbLIC::SDN1gs (Appendix Table S3). For agroinfiltration, four constructs (pCaBS-α, pCaBS-β, pCa-γbLIC, and pCa-γbLIC::SDN1gs) were individually transformed into the *Agrobacterium* strain EHA105 (Biomed). After incubation at room temperature for 3 h, the suspended *Agrobacterium* cells carrying pCaBS-α, pCaBS-β, or pCa-γbLIC were mixed at a ratio of 1:1:1, and infiltrated into *N. benthamiana* leaves, which reconstituted the empty vector control (BSMV-EV). Similarly, the *Agrobacterium* cells carrying pCaBS-α, pCaBS-β, or pCa-γbLIC::SDN1gs were mixed, and infiltrated into *N. benthamiana* leaves, which formed the silencing inducing virus (BSMV-SDN1gs). The *N. benthamiana* leaves exhibited BSMV infection symptom at about 12-day post infiltration. The leaves of the tobaccos infected by BSMV-EV or BSMV-SDN1gs were each grinded in Na-phosphate buffer (containing 1% celite, pH 7.2). The resultant sap was used to inoculate the barley seedlings at two-leaf stage. For both BSMV-EV and BSMV-SDN1gs, 150 barley seedlings were inoculated.

The barley plants were analyzed at 2-week post inoculation with BSMV-SDN1gs or BSMV-EV to assess the silencing of *HvSDN1* expression as described previously (Jin et al, 2020). Then, the plants infected by BSMV-SDN1gs or BSMV-EV were each divided into two groups. One group ( $n \geq 30$ ) was further inoculated with BYDV using viruliferous aphids. The other group ( $n \geq 30$ ) was

treated with virus-free *Schizaphis graminum* and kept as controls. This produced four groups of barley plants, that is, BSMV-EV/BYDV<sup>-</sup> (without *HvSDN1* silencing and free of BYDV-GAV), BSMV-SDN1gs/BYDV<sup>-</sup> (with *HvSDN1* silenced and free of BYDV-GAV), BSMV-EV/BYDV<sup>+</sup> (without *HvSDN1* silencing and infected by BYDV-GAV), and BSMV-SDN1gs/BYDV<sup>+</sup> (with *HvSDN1* silenced and infected by BYDV-GAV). The four groups of plants were examined for changes in morphology, plant height, and accumulation of viral transcripts at 3-week post-BYDV inoculation. The accumulation of BYDV in the BSMV-EV/BYDV<sup>+</sup> and BSMV-SDN1gs/BYDV<sup>+</sup> plants was detected by qRT-PCR assay of CP transcripts with specific primers, with the amplification of barley *Actin* gene as an internal control (Appendix Table S2).

### Genome editing of *TaSDN1*

Genome editing of *TaSDN1* in common wheat was conducted as described previously (Wang *et al*, 2014). Briefly, the sgRNA, specifically targeting the three *TaSDN1* homoeologs (Fig EV5H), was synthesized (Beijing SYKM Gene Biotechnology Co. Ltd.) and cloned into the pZCRISPR/Cas9<sub>ubi</sub> vector, which was then used to transform the immature embryos of the common wheat cultivar Fielder. A total of three separate genome editing experiments were accomplished, which yielded 273 T<sub>0</sub> transformations. These T<sub>0</sub> plants were individually genotyped using PCR-RE analysis, followed by Sanger sequencing of the amplicons produced by PCR with the primer sets (Appendix Table S2) specific for each homoeolog (*TaSDN1-A*, *-B*, or *-D*). Only one heterozygous mutant, *TaSDN1-Dd*, was identified, which was used to create a wheat population segregating for *TaSDN1-DD*, *TaSDN1-Dd*, and *TaSDN1-dd* genotypes through repeated selfing of *TaSDN1-Dd* individuals. *HvSDN1* protein level in the three genotypes was analyzed using an anti-*HvSDN1* antibody prepared in this work (Fig EV4E). The segregating population was then inoculated with BYDV ( $\geq 30$  plants inoculated for each genotype), with disease symptoms, expression of viral CP, and accumulation of vsRNAs evaluated as described above.

### Quantification of gel band intensity

Relative intensities of protein or vsRNA bands were obtained using the ImageJ software (<https://imagej.nih.gov/ij/index.html>).

### Statistical analysis

Statistical analysis of the data, presented as means  $\pm$  standard deviation (SD), was conducted using either Student's *t*-test (for pairwise comparisons) or a combination of one-way ANOVA and least significant difference test (LSD, for multiple comparisons) installed in the SPSS program (SPSS Inc., Chicago, IL, USA).

### Accession numbers

The nucleic acid sequences used in this work can be found in the databases of GenBank, *Arabidopsis* Genome Initiative or Ensemble Plant with the following accession numbers: NC\_004666 (barley yellow dwarf virus-GAV), NC\_002036 (Pea early browning virus, genome RNA 1), NC\_001368 (Pea early browning virus, genome RNA 2), AB910929 (barley SnRK1), AK368039 (barley GRIK1),

AK373112 (barley AGO1), HORVU2Hr1G113320 (barley SDN1), HORVU3Hr1G075890 (barley SDN5), TraesCS2A02G510900 (wheat SDN1-A), TraesCS2B02G538900 (wheat SDN1-B), TraesCS2D02G512200 (wheat SDN1-D), TraesCS3A02G320700 (wheat SDN5-A), TraesCS3B02G345100 (wheat SDN5-B), TraesCS3D02G310600 (wheat SDN5-D), AT3G50100 (*Arabidopsis* SDN1), AT5G05540 (*Arabidopsis* SDN2), AT5G67240 (*Arabidopsis* SDN3), AT3G50090 (*Arabidopsis* SDN4), AT5G25800 (*Arabidopsis* SDN5), NP\_056750 (PLRV 17K), XP\_044968114 (barley PKABA1), BAJ97011 (barley CIPK1).

## Data availability

The sRNA sequencing data have been deposited in GenBank under the accession numbers PRJNA823841 (<http://www.ncbi.nlm.nih.gov/bioproject/823841>), PRJNA823874 (<http://www.ncbi.nlm.nih.gov/bioproject/823874>), and PRJNA823894 (<http://www.ncbi.nlm.nih.gov/bioproject/823894>), respectively.

**Expanded View** for this article is available online.

### Acknowledgments

We thank Professor Jörg Kudla for providing the TriFC constructs and Professors Jinlong Qiu (Chinese Academy of Sciences) and Dawei Li and Yongliang Zhang (China Agricultural University) for constructive advice on manuscript writing. This work was supported by the Key Science and Technology Program of Henan Province (201300110800 to DW), Zhongyuan Thousand Talents Program (ZYQR201912168 to MG), and the Postdoctoral Science Foundations of China (2020M672231 to HJ) and Henan Province (201902032 to HJ).

### Author contributions

**Daowen Wang:** Conceptualization; resources; data curation; formal analysis; supervision; funding acquisition; visualization; methodology; writing – original draft; project administration; writing – review and editing. **Huaibing Jin:** Conceptualization; formal analysis; funding acquisition; validation; investigation; visualization; methodology; writing – original draft; project administration; writing – review and editing. **Xinyun Han:** Resources; investigation; methodology. **Zhaohui Wang:** Resources; validation; investigation; methodology. **Yilin Xie:** Formal analysis; validation; investigation. **Kunpu Zhang:** Investigation. **Xiaoge Zhao:** Investigation. **Lina Wang:** Investigation. **Jin Yang:** Methodology. **Huiyun Liu:** Resources. **Xiang Ji:** Resources. **Lingli Dong:** Methodology. **Hongyuan Zheng:** Investigation. **Weijuan Hu:** Resources. **Yan Liu:** Resources. **Xifeng Wang:** Resources. **Xueping Zhou:** Resources. **Yijing Zhang:** Supervision. **Weiqliang Qian:** Supervision. **Wenming Zheng:** Investigation. **Qianhua Shen:** Resources; supervision. **Mingyue Gou:** Funding acquisition.

### Disclosure and competing interests statement

The authors declare that they have no conflict of interest.

## References

- Ali M, Anwar S, Shuja MN, Tripathi RK, Singh J (2018) The genus *Luteovirus* from infection to disease. *Eur J Plant Pathol* 151: 841–860
- Annacondia ML, Martinez G (2021) Reprogramming of RNA silencing triggered by cucumber mosaic virus infection in *Arabidopsis*. *Genome Biol* 22: 340

- Aradottir GI, Crespo-Herrera L (2021) Host plant resistance in wheat to barley yellow dwarf viruses and their aphid vectors: a review. *Curr Opin Insect Sci* 45: 59–68
- Baulcombe D (2004) RNA silencing in plants. *Nature* 431: 356–363
- Bortolamiol D, Pazhouhandeh M, Marrocco K, Genschik P, Ziegler-Graff V (2007) The Ploverovirus F box protein PO targets ARGONAUTE1 to suppress RNA silencing. *Curr Biol* 17: 1615–1621
- Bronkhorst AW, Vogels R, Overheul GJ, Pennings B, Gausson-Dorey V, Miesen P, van Rij RP (2019) A DNA virus-encoded immune antagonist fully masks the potent antiviral activity of RNAi in *Drosophila*. *Proc Natl Acad Sci USA* 116: 24296–24302
- Chen H, Zou Y, Shang Y, Lin H, Wang Y, Cai R, Tang X, Zhou JM (2008) Firefly luciferase complementation imaging assay for protein-protein interactions in plants. *Plant Physiol* 146: 368–376
- Chen J, Liu L, You C, Gu J, Ruan W, Zhang L, Gan J, Cao C, Huang Y, Chen X et al (2018) Structural and biochemical insights into small RNA 3' end trimming by *Arabidopsis* SDN1. *Nat Commun* 9: 3585
- Chen S, Han X, Yang L, Li Q, Shi Y, Li H, Chen L, Sun B, Shi Y, Yang X (2021a) Identification and functional analyses of host factors interacting with the 17-kDa protein of barley yellow dwarf virus-GAV. *Sci Rep* 11: 8453
- Chen Z, Zhou L, Jiang P, Lu R, Halford NG, Liu C (2021b) Genome-wide identification of sucrose nonfermenting-1-related protein kinase (SnRK) genes in barley and RNA-seq analyses of their expression in response to abscisic acid treatment. *BMC Genomics* 22: 300
- Cho YH, Hong JW, Kim EC, Yoo SD (2012) Regulatory functions of SnRK1 in stress-responsive gene expression and in plant growth and development. *Plant Physiol* 158: 1955–1964
- Clavel M, Lechner E, Incarbone M, Vincent T, Cognat V, Smirnova E, Lecorbeiller M, Brault V, Ziegler-Graff V, Genschik P (2021) Atypical molecular features of RNA silencing against the phloem-restricted polerovirus TuYV. *Nucleic Acids Res* 49: 11274–11293
- Constantin GD, Krath BN, MacFarlane SA, Nicolaisen M, Johansen IE, Lund OS (2004) Virus-induced gene silencing as a tool for functional genomics in a legume species. *Plant J* 40: 622–631
- Csorba T, Lózsza R, Hutvágner G, Burgyán J (2010) Ploverovirus protein PO prevents the assembly of small RNA-containing RISC complexes and leads to degradation of ARGONAUTE1. *Plant J* 62: 463–472
- Emanuelle S, Doblin MS, Stapleton DI, Bacic A, Gooley PR (2016) Molecular insights into the enigmatic metabolic regulator, SnRK1. *Trends Plant Sci* 21: 341–353
- Fang X, Qi Y (2016) RNAi in plants: an Argonaute-centered view. *Plant Cell* 28: 272–285
- Fernández-Calvino L, Martínez-Priego L, Szabo EZ, Guzmán-Benito I, González I, Canto T, Lakatos L, Llave C (2016) Tobacco rattle virus 16K silencing suppressor binds ARGONAUTE 4 and inhibits formation of RNA silencing complexes. *J Gen Virol* 97: 246–257
- Feys BJ, Wiermer M, Bhat RA, Moisan LJ, Medina-Escobar N, Neu C, Cabral A, Parker JE (2005) *Arabidopsis* SENESCENCE-ASSOCIATED GENE101 stabilizes and signals within an ENHANCED DISEASE SUSCEPTIBILITY1 complex in plant innate immunity. *Plant Cell* 17: 2601–2613
- Fire A, Xu S, Montgomery MK, Kostas SA, Driver SE, Mello CC (1998) Potent and specific genetic interference by double-stranded RNA in *Caenorhabditis elegans*. *Nature* 391: 806–811
- Fusaro AF, Barton DA, Nakasugi K, Jackson C, Kalischuk ML, Kawchuk LM, Vaslin MFS, Correa RL, Waterhouse PM (2017) The luteovirus P4 movement protein is a suppressor of systemic RNA silencing. *Viruses* 9: 294
- García-Ruiz H, Carbonell A, Hoyer JS, Fahlgren N, Gilbert KB, Takeda A, Giampetruzzi A, García Ruiz MT, McGinn MG, Lowery N et al (2015) Roles and programming of *Arabidopsis* ARGONAUTE proteins during turnip mosaic virus infection. *PLoS Pathog* 11: e1004755
- Goulden MG, Lomonosoff GP, Davies JW, Wood KR (1990) The complete nucleotide sequence of PEBV RNA2 reveals the presence of a novel open reading frame and provides insights into the structure of tobamovirus subgenomic promoters. *Nucleic Acids Res* 18: 4507–4512
- Guo Z, Li Y, Ding SW (2019) Small RNA-based antimicrobial immunity. *Nat Rev Immunol* 19: 31–44
- Halford NG, Grahame Hardie D (1998) SNF1-related protein kinases: global regulators of carbon metabolism in plants? *Plant Mol Biol* 37: 735–748
- Halford NG, Hey SJ (2009) Snf1-related protein kinases (SnRKs) act within an intricate network that links metabolic and stress signaling in plants. *Biochem J* 419: 247–259
- Han Q, Chen G, Wang J, Jee D, Li WX, Lai EC, Ding SW (2020a) Mechanism and function of antiviral RNA interference in mice. *mBio* 11: e03278-19
- Han X, Zhang L, Zhao L, Xue P, Qi T, Zhang C, Yuan H, Zhou L, Wang D, Qiu J et al (2020b) SnRK1 phosphorylates and destabilizes WRKY3 to enhance barley immunity to powdery mildew. *Plant Commun* 1: 100083
- Hao L, Wang H, Sunter G, Bisaro DM (2003) Geminivirus AL2 and L2 proteins interact with and inactivate SNF1 kinase. *Plant Cell* 15: 1034–1048
- Heck M, Brault V (2018) Targeted disruption of aphid transmission: a vision for the management of crop diseases caused by *Luteoviridae* members. *Curr Opin Virol* 33: 24–32
- Hernandez-Gonzalez M, Larocque G, Way M (2021) Viral use and subversion of membrane organization and trafficking. *J Cell Sci* 134: jcs252676
- Holappa LD, Walker-Simmons MK (1995) The wheat abscisic acid-responsive protein kinase mRNA, PKABA1, is up-regulated by dehydration, cold temperature, and osmotic stress. *Plant Physiol* 108: 1203–1210
- Hrabak EM, Chan CW, Gribskov M, Harper JF, Choi JH, Halford N, Kudla J, Luan S, Nimmo HG, Sussman MR et al (2003) The *Arabidopsis* CDPK-SnRK superfamily of protein kinases. *Plant Physiol* 132: 666–680
- Huang YW, Hu CC, Tsai CH, Lin NS, Hsu YH (2019) *Nicotiana benthamiana* Argonaute10 plays a pro-viral role in bamboo mosaic virus infection. *New Phytol* 224: 804–817
- Hulsmans S, Rodriguez M, De Coninck B, Rolland F (2016) The SnRK1 energy sensor in plant biotic interactions. *Trends Plant Sci* 21: 648–661
- Iki T, Tschopp MA, Voinnet O (2017) Biochemical and genetic functional dissection of the P38 viral suppressor of RNA silencing. *RNA* 23: 639–654
- Jin Z, Wang X, Chang S, Zhou G (2004) The complete nucleotide sequence and its organization of the genome of barley yellow dwarf virus-GAV. *Sci China C Life Sci* 47: 175–182
- Jin H, Du Z, Zhang Y, Antal J, Xia Z, Wang Y, Gao Y, Zhao X, Han X, Cheng Y et al (2020) A distinct class of plant and animal viral proteins that disrupt mitosis by directly interrupting the mitotic entry switch Wee1-Cdc25-Cdk1. *Sci Adv* 6: eaba3418
- Kinoshita E, Kinoshita-Kikuta E, Kubota Y, Takekawa M, Koike T (2016) A Phos-tag SDS-PAGE method that effectively uses phosphoproteomic data for profiling the phosphorylation dynamics of MEK1. *Proteomics* 16: 1825–1836
- Lakatos L, Szittya G, Silhavy D, Burgyán J (2004) Molecular mechanism of RNA silencing suppression mediated by p19 protein of tombusviruses. *EMBO J* 23: 876–884
- Lakatos L, Csorba T, Pantaleo V, Chapman EJ, Carrington JC, Liu YP, Dolja VV, Calvino LF, López-Moya JJ, Burgyán J (2006) Small RNA binding is a common strategy to suppress RNA silencing by several viral suppressors. *EMBO J* 25: 2768–2780

- Li F, Wang A (2019) RNA-targeted antiviral immunity: more than just RNA silencing. *Trends Microbiol* 27: 792–805
- Link K, Vogel F, Sonnewald U (2011) PD trafficking of potato leaf roll virus movement protein in *Arabidopsis* depends on site-specific protein phosphorylation. *Front Plant Sci* 2: 18
- Martínez-Barajas E, Coello P (2020) Review: how do SnRK1 protein kinases truly work? *Plant Sci* 291: 110330
- Miller WA, Rasochová L (1997) Barley yellow dwarf viruses. *Annu Rev Phytopathol* 35: 167–190
- Nass PH, Domier LL, Jakstys BP, D'Arcy CJ (1998) *In situ* localization of barley yellow dwarf virus-PAV 17-kDa protein and nucleic acids in oats. *Phytopathology* 88: 1031–1039
- Offenborn JN, Waadt R, Kudla J (2015) Visualization and translocation of ternary calcineurin-a/calcineurin-B/Calmodulin-2 protein complexes by dual-color trimolecular fluorescence complementation. *New Phytol* 208: 269–279
- Pertermann R, Tamilarasan S, Gursinsky T, Gambino G, Schuck J, Weinholdt C, Lilie H, Grosse I, Golbik RP, Pantaleo V et al (2018) A viral suppressor modulates the plant immune response early in infection by regulating microRNA activity. *mBio* 9: e00419-18
- Ramachandran V, Chen X (2008) Degradation of microRNAs by a family of exoribonucleases in *Arabidopsis*. *Science* 321: 1490–1492
- de Ronde D, Butterbach P, Lohuis D, Hedil M, van Lent JW, Kormelink R (2013) Tsw gene-based resistance is triggered by a functional RNA silencing suppressor protein of the tomato spotted wilt virus. *Mol Plant Pathol* 14: 405–415
- Shen W, Hanley-Bowdoin L (2020) SnRK1: a versatile plant protein kinase that limits geminivirus infection. *Curr Opin Virol* 47: 18–24
- Shen W, Reyes MI, Hanley-Bowdoin L (2009) *Arabidopsis* protein kinases GRIK1 and GRIK2 specifically activate SnRK1 by phosphorylating its activation loop. *Plant Physiol* 150: 996–1005
- Shen M, Xu Y, Jia R, Zhou X, Ye K (2010) Size-independent and noncooperative recognition of dsRNA by the rice stripe virus RNA silencing suppressor NS3. *J Mol Biol* 404: 665–679
- Shen Q, Liu Z, Song F, Xie Q, Hanley-Bowdoin L, Zhou X (2011) Tomato SlSnRK1 protein interacts with and phosphorylates  $\beta$ C1, a pathogenesis protein encoded by a geminivirus  $\beta$ -satellite. *Plant Physiol* 157: 1394–1406
- Shen W, Dallas MB, Goshe MB, Hanley-Bowdoin L (2014) SnRK1 phosphorylation of AL2 delays cabbage leaf curl virus infection in *Arabidopsis*. *J Virol* 88: 10598–10612
- Shen W, Bobay BG, Greeley LA, Reyes MI, Rajabu CA, Blackburn RK, Dallas MB, Goshe MB, Ascencio-Ibáñez JT, Hanley-Bowdoin L (2018) Sucrose non-fermenting 1-related protein kinase 1 phosphorylates a geminivirus rep protein to impair viral replication and infection. *Plant Physiol* 178: 372–389
- Shen C, Wei C, Li J, Zhang X, Zhong Q, Li Y, Bai B, Wu Y (2020) Barley yellow dwarf virus-GAV-derived vsRNAs are involved in the production of wheat leaf yellowing symptoms by targeting chlorophyll synthase. *Virology* 531: 158
- Silva TF, Romanel EA, Andrade RR, Farinelli L, Østerås M, Deluen C, Corrêa RL, Schrago CE, Vaslin MF (2011) Profile of small interfering RNAs from cotton plants infected with the polerovirus cotton leafroll dwarf virus. *BMC Mol Biol* 12: 40
- Smirnova E, Firth AE, Miller WA, Scheidecker D, Brault V, Reinbold C, Rakotondrafara AM, Chung BY, Ziegler-Graff V (2015) Discovery of a small non-AUG initiated ORF in poleroviruses and luteoviruses that is required for long-distance movement. *PLoS Pathog* 11: e1004868
- Tacke E, Schmitz J, Prüfer D, Rohde W (1993) Mutational analysis of the nucleic acid-binding 17 kDa phosphoprotein of potato leafroll luteovirus identifies an amphipathic alpha-helix as the domain for protein/protein interactions. *Virology* 197: 274–282
- Valli AA, Gallo A, Rodamilans B, López-Moya JJ, García JA (2018) The HCPro from the Potyviridae family: an enviable multitasking helper component that every virus would like to have. *Mol Plant Pathol* 19: 744–763
- Vargason JM, Szittyá G, Burgyán J, Hall TM (2003) Size selective recognition of siRNA by an RNA silencing suppressor. *Cell* 115: 799–811
- Walsh D, Mohr I (2011) Viral subversion of the host protein synthesis machinery. *Nat Rev Microbiol* 9: 860–875
- Wang D, Maule AJ (1997) Contrasting patterns in the spread of two seed-borne viruses in pea embryos. *Plant J* 11: 1333–1340
- Wang H, Hao L, Shung CY, Sunter G, Bisaro DM (2003) Adenosine kinase is inactivated by geminivirus AL2 and L2 proteins. *Plant Cell* 15: 3020–3032
- Wang X, Liu Y, Chen L, Zhao D, Wang X, Zhang Z (2013) Wheat resistome in response to barley yellow dwarf virus infection. *Funct Integr Genomics* 13: 155–165
- Wang Y, Cheng X, Shan Q, Zhang Y, Liu J, Gao C, Qiu JL (2014) Simultaneous editing of three homoeoalleles in hexaploid bread wheat confers heritable resistance to powdery mildew. *Nat Biotechnol* 32: 947–951
- Wang K, Liu H, Du L, Ye X (2017) Generation of marker-free transgenic hexaploid wheat via an agrobacterium-mediated co-transformation strategy in commercial Chinese wheat varieties. *Plant Biotechnol J* 15: 614–623
- Xia Z, Wang Y, Du Z, Li J, Zhao R, Wang D (2008) A potential nuclear envelope-targeting domain and an arginine-rich RNA binding element identified in the putative movement protein of the GAV strain of barley yellow dwarf virus. *Funct Plant Biol* 35: 40–50
- Yaegashi H, Isogai M, Yoshikawa N (2012) Characterization of plant virus-encoded gene silencing suppressors. *Methods Mol Biol* 894: 113–122
- Yu Y, Ji L, Le BH, Zhai J, Chen J, Luscher E, Gao L, Liu C, Cao X, Mo B et al (2017) Argonaute10 promotes the degradation of miR165/6 through the SDN1 and SDN2 exonucleases in *Arabidopsis*. *PLoS Biol* 15: e2001272
- Yuan C, Li C, Yan L, Jackson AO, Liu Z, Han C, Yu J, Li D (2011) A high throughput barley stripe mosaic virus vector for virus induced gene silencing in monocots and dicots. *PLoS One* 6: e26468
- Zhang X, Dong K, Xu K, Zhang K, Jin X, Yang M, Zhang Y, Wang X, Han C, Yu J et al (2018) Barley stripe mosaic virus infection requires PKA-mediated phosphorylation of  $\gamma$ b for suppression of both RNA silencing and the host cell death response. *New Phytol* 218: 1570–1585
- Zhang L, Xu W, Gao X, Li W, Qi S, Guo D, Ajayi OE, Ding SW, Wu Q (2020) LncRNA sensing of a viral suppressor of RNAi activates non-canonical innate immune signaling in *Drosophila*. *Cell Host Microbe* 27: 115–128
- Zhang X, Wang X, Xu K, Jiang Z, Dong K, Xie X, Zhang H, Yue N, Zhang Y, Wang XB et al (2021) The serine/threonine/tyrosine kinase STY46 defends against hordeivirus infection by phosphorylating  $\gamma$ b protein. *Plant Physiol* 186: 715–730
- Zhong X, Wang Z, Xiao R, Cao L, Wang Y, Xie Y, Zhou X (2017) Mimic phosphorylation of a  $\beta$ C1 protein encoded by TYLCCNB impairs its functions as a viral suppressor of RNA silencing and a symptom determinant. *J Virol* 91: e00300-17



**License:** This is an open access article under the terms of the [Creative Commons Attribution-NonCommercial-NoDerivs](https://creativecommons.org/licenses/by-nc-nd/4.0/) License, which permits use and distribution in any medium, provided the original work is properly cited, the use is noncommercial and no modifications or adaptations are made.